Ensemble Kalman inversion for sparse learning of dynamical systems from time-averaged data

Tapio Schneider, Andrew M. Stuart, Jin-Long Wu [*]

California Institute of Technology, Pasadena, CA 91125, United States of America

A B S T R A C T

Enforcing sparse structure within learning has led to significant advances in the field of data-driven discovery of dynamical systems. However, such methods require access not only to timeseries of the state of the dynamical system, but also to the time derivative. In many applications, the data are available only in the form of time-averages such as moments and autocorrelation functions. We propose a sparse learning methodology to discover the vector fields defining a (possibly stochastic or partial) differential equation, using only time-averaged statistics. Such a formulation of sparse learning naturally leads to a nonlinear inverse problem to which we apply the methodology of ensemble Kalman inversion (EKI). EKI is chosen because it may be formulated in terms of the iterative solution of quadratic optimization problems; sparsity is then easily imposed. We then apply the EKI-based sparse learning methodology to various examples governed by stochastic differential equations (a noisy Lorenz 63 system), ordinary differential equations (Lorenz 96 system and coalescence equations), and a partial differential equation (the Kuramoto-Sivashinsky equation). The results demonstrate that time-averaged statistics can be used for data-driven discovery of differential equations using sparse EKI. The proposed sparse learning methodology extends the scope of data-driven discovery of differential equations to previously challenging applications and data-acquisition scenarios.

© 2022 Elsevier Inc. All rights reserved.

1. Introduction

1.1. Overview and literature review

The goal of this paper is to describe a sparse learning methodology to discover the vector fields defining a (possibly stochastic or partial) differential equation, using timeseries data. The approach is to use ensemble Kalman inversion (EKI) to learn the unknown vector fields by matching the model to time-averaged statistics derived from the timeseries data. Sparse learning allows for the discovery of dynamical models from within a large dictionary of models. Learning from time-averaged statistics is often necessary either because data are available only in that form, or because use of time-averages avoids incompatibility issues between model and data at small time increments and the lack of differentiability of sample paths of stochastic differential equations (SDEs). The EKI methodology is an approach to parameter identification that lends itself naturally to the imposition of constraints such as sparsity, and that has proven empirically to be robust and flexible. The work presented here leads to a new approach that widens the scope of sparse learning problems in dynamical systems,

---

by allowing for data in the form of time averages. The approach is both flexible (applying to a range of examples) and robust (works very well in practice). Our work suggests wider deployment of the proposed methodology, and the need for development of an underpinning theory.

Seeking sparse structure in learning has played a significant role in recent decades. Sparse dictionary learning techniques are well known as compressed sensing [1–3] and have already been extensively studied in application domains such as image and signal processing [4]. The general concept of incorporating sparsity into optimization has also been studied in a variety of applied disciplines for several decades, for example in applications in geophysics [5]. Since then it has been formulated within a theoretical framework known as LASSO [6,7]. In addition, sparsity-promoting techniques have been found useful in emerging areas in artificial intelligence, such as deep learning [8].

Exploitation of sparsity in the data-driven discovery of differential equations was pioneered in a recent series of papers [9–12], all of which make the assumption that the vector fields to be discovered are sparse within a high-dimensional dictionary. More recently, a sparsity-promoting joint outlier detection and model discovery method was proposed in [13], and a sparsity-promoting method was proposed in [14] for learning governing equations of dynamical systems from under-sampled data. These methods need to be provided with, or need to numerically evaluate, timeseries of the time derivative of the state variables, as well as the timeseries of state variables themselves. The data-driven discovery of differential equations with sparsity has also been investigated for the learning of stochastic differential equations [15,16]; in this setting the time-derivative is not required – indeed it does not exist – but Itô integrals with respect to the timeseries must be evaluated. In such settings, the learning problem results in an over-determined system of linear equations, and the solution may be sought through a regularized least squares approach in which the regularization imposes sparsity. When numerical differentiation is required, it is susceptible to noise in the timeseries of the state variables. Techniques such as total variation regularization [17] have been adopted to alleviate this issue by denoising the time derivative [18]. Nonetheless, the presence of noise in timeseries presents a significant issue for these approaches.

One way of circumventing the need to numerically differentiate timeseries is to fit dynamical models to statistics derived from timeseries, such as moments or autocorrelation functions. This idea is widely used in the study of autoregressive (AR) processes [19–24] and in the study of SDEs [25–29]. There is also a plethora of applied papers that take this approach, in both discrete and continuous time, such as [30,31]. In addition to avoiding numerical differentiation, such methods have the potential to learn models when only a subset of the state variables is observed. Furthermore, there are settings in which only time-averaged data are available. It is important to note that the parameter-to-data map for such problems can be nonlinear.

In this work, we propose a sparsity-promoting methodology for parameter learning, within the context of ensemble Kalman methods [32]. Ensemble Kalman methods are well-adapted to the solution of nonlinear inverse problems when the forward model is provided as a black box, and is potentially hard or expensive to differentiate. In previous papers [33,34], ensemble Kalman methods were developed for the solution of general inverse problems, generalizing the methodology beyond the setting of state estimation where it was originally introduced [35,36]. The paper [37] connected ensemble methods with sequential Monte Carlo methods for Bayesian inverse problems, and discussed their use for optimization as opposed to Bayesian inversion. Ensemble Kalman methods are formulated as an optimization approach to general inverse problems in [38]. We refer to this ensemble based optimization methodology, and its continuous time analogue analyzed in [39], as ensemble Kalman inversion (EKI). The use of ensemble Kalman methods to learn dynamical systems is discussed in [40,41], and the use of EKI to learn dynamical systems from time-averaged data is discussed in [29]. Incorporation of constraints into ensemble Kalman methods is studied in [42–48]. The sparse version of the EKI approach that we propose here combines ideas from [38,42,43] to create a derivative-free optimization approach to parameter learning that enforces sparsity.

In [49] an approach to regularizing EKI in the ℓ_p was proposed; the method proceeds by first transforming the ℓ_p constraint (for $0 < p \leq 1$) into an ℓ_2 constraint, and then solving using Tikhonov-regularized EKI [44]. In contrast our approach is focused specifically on the ℓ_1 constraint and operates by transforming the problem to a standard convex optimization problem, which can be solved efficiently by use of standard software. While our approach is not as general as that proposed in [49], it avoids the measurement augmentation needed to implement Tikhonov-regularized EKI and this can be expensive when the dimension of the unknown parameter space is large. By explicitly formulating a convex optimization problem, we can also utilize existing approaches to regularize the standard optimization problem, such as the operator splitting approach introduced in [12]; this may be important when employing a relative small ensemble size. Our approach formulates methodology based on the combined use of an ℓ_1 constraint and thresholding, in the context of EKI, and makes links with thresholding and ℓ_0 constraint.

We apply the method to the learning of vector fields in (possibly stochastic or partial) differential equations, building on the ideas in [9], but using nonlinear indirect measurements defined by time-averaging, rather than linear direct observations. It is a remarkable property of EKI that, despite the nonlinearity of the observation operator, the core computational task (which must be tackled several times as part of an outer iteration and for each ensemble member) is the minimization of a quadratic objective functional to which a sparsity constraint may be easily added, just as it is in the original work on sparse learning of dynamical systems in [9]. This fact allows transfer of the learning framework introduced in [9] to more complex, indirectly, nonlinearly and partially observed dynamics, and indeed to a wide range of nonlinear inverse and parameter identification problems. Our motivation is in part to introduce the methodology as a way of learning about structural errors in complex computer models, such as climate models [50].

1.2. Our contribution

Our contributions in this paper are as follows:

- We demonstrate how to impose a sparsity constraint within the EKI algorithm, by formulating the update step as an ℓ_1 and/or ℓ_0 regularized least squares problem.
- We demonstrate the use of sparsity-promoting EKI to discover the governing equations of (possibly stochastic) dynamical systems based on statistics derived from averaging timeseries. The results are compared with those obtained using standard EKI to illustrate the merits of imposing sparsity.
- We illustrate the methodology in two simulation studies, discovering the stochastic Lorenz '63 and the deterministic Lorenz '96 systems from data, and we also illustrate the methodology to find a closure model for the slow variables within a multiscale Lorenz '96 system.
- We illustrate the methodology by discovering coalescence equations for collisional dynamics, using both simulation studies and closure models.
- We illustrate the methodology in the context of discovering the Kuramoto-Sivashinsky equation from a larger family of semilinear dissipative and dispersive systems, in the presence of energy conserving quadratic nonlinearities.
- We demonstrate how to impose constraints on the parameter learning that ensure that the subset of parameters that are queried during the algorithm all lead to well-posed dynamical systems.

We emphasize that, although we apply the method in the context of learning dynamical systems, the sparse EKI-based methodology may be more widely applied to quite general nonlinear inverse problems.

In Section 2, we formulate the inverse problem of interest and introduce the four problem classes to which we will apply our methodology. Section 3 describes the ensemble Kalman-based methodology that we employ to solve the inverse problem; we also discuss the quadratic programming approach we employ to incorporate the ℓ_1-penalty into the ensemble Kalman-based methodology, and the proximal gradient methodology used to incorporate the ℓ_0-penalty. In Section 4, we describe numerical results relating to each of the four example problems. We conclude in Section 5.

1.3. Notation

We use $|\cdot|_{\ell_p}$ to denote the p-norm in Euclidean space, extended to include the case $p = 0$, which counts the number of non-zero entries of the vector. The commonly occurring case $p = 2$ is simply denoted by $|\cdot|$, and the notation $|\cdot|_A := |A^{-\frac{1}{2}}\cdot|$ is used for symmetric positive-definite A.

2. Problem formulation

The aim of this work is to use timeseries data to learn the right hand side of a differential equation

$$\frac{dx}{dt} = f(x), \tag{2.1}$$

where $x \in \mathbb{R}^n$ and $f : \mathbb{R}^n \mapsto \mathbb{R}^n$, from time-averaged information about x. To this end, we first approximate f with a set of basis functions $\phi = \{\phi_i\}$, $i \in \{1, ..., p\}$, leading to a modeled differential equation

$$\frac{dX_k}{dt} = \sum_{i=1}^{p} \theta_{ki}\phi_i(X), \quad k = 1, ..., n, \tag{2.2}$$

where $X \in \mathbb{R}^n$ has components X_k, $\phi_i : \mathbb{R}^n \mapsto \mathbb{R}$, and the parameter matrix is $\theta \in \Theta \subseteq \mathbb{R}^{n \times p}$. We assume that, with appropriate choice of the basis functions $\{\phi_i\}$, the function $X(t)$ provides a good approximation of $x(t)$ for some choice of parameter matrix θ; furthermore, we assume that this choice of θ is sparse in the sense that $|\theta|_{\ell_0} \ll np$. We will also consider generalizations to SDEs and to partial differential equations (PDEs).

We assume that the data y are available to us in the form of time-averages of quantities derived from $x(t)$, or linear transformations of such quantities. This includes moments, autocorrelation functions, and the power spectral density. If $x(\cdot)$ and $X(\cdot; \theta) \in \mathcal{X} := C(\mathbb{R}^+, \mathbb{R}^n)$ denote solutions of the true and modeled systems, Θ denotes the subset of parameter space over which we seek modeled solutions, and $\mathcal{F} : \mathcal{X} \mapsto \mathbb{R}^J$ is a function on the space of solution trajectories, then define $\mathcal{G}(\theta) := \mathcal{F}(X(\cdot; \theta)) : \Theta \mapsto \mathbb{R}^J$. In this work, $\mathcal{F}$ corresponds to time-averaged functions of solution trajectories $x(\cdot)$. We focus on solution of the following inverse problem to determine θ from y:

$$y = \mathcal{G}(\theta). \tag{2.3}$$

For simplicity, we have assumed independence of $\mathcal{G}$ from the initial condition (and the driving Brownian noise in the SDE case), noting that for ergodic problems this dependence indeed disappears when time-averages over the infinite time

horizon are used. In practice, a noisy finite-time average is used to generate the data, and the resulting fluctuations may be viewed as small noise around the infinite time average. We will account for this in our algorithms. The ergodic setting will obtain for most of the examples considered in this paper. However, one of the examples we study is not ergodic (the coalescence equations), and in that setting we study the dependence of our learned parameters on the initial condition.

The formulation in Eq. (2.3) has the advantage that it does not involve the matching of trajectories $x(t)$ and $X(t)$, a problem that can be difficult when noise is present in the data (for example, from using finite-time rather than ergodic averages) or when the trajectory is not differentiable (as arises in SDEs). However, the approach we adopt has the apparent disadvantage that the data available may be of small volume. Indeed, it may be the case that $J \ll np$ – that is, the amount of data is far less than the number of unknowns. Nonetheless, a sparse solution for θ often provides a better modeled system than a dense one and can still be identifiable with limited data. Therefore, we aim to solve the inverse problem formulated in Eq. (2.3) by using a modified version of ensemble Kalman inversion (EKI) that promotes sparsity in θ.

We now describe four examples that we use to illustrate the methodology. In all four cases, we demonstrate how to ensure that parameter learning takes place within a subset of parameter models that lead to well-posed dynamics. For the EKI approach adopted here, it is integral to the method that the candidate model problems are simulated for a variety of parameter values during the learning algorithm, and the resulting outputs are compared with the data available. This ensures that the candidate parameter values lead to well-posed dynamics. The reader primarily interested in the form of the algorithm can skip straight to Section 3 and return to the following examples in conjunction with reading Section 4.

Example 2.1 (*Lorenz 63 System [51]*). The noisy Lorenz equations are a system of three ordinary differential equations taking the form

$$\dot{x} = f(x) + \sqrt{\sigma^{\dagger}}\dot{W}, \tag{2.4}$$

where W is an $\mathbb{R}^3$-valued Brownian motion, $x = [x_1, x_2, x_3]^{\top}$, and $f : \mathbb{R}^3 \mapsto \mathbb{R}^3$ is given by

$$\begin{aligned} f_1(x) &= \alpha(x_2 - x_1), \\ f_2(x) &= x_1(\rho - x_3) - x_2, \\ f_3(x) &= x_1 x_2 - \beta x_3. \end{aligned} \tag{2.5}$$

We will seek a modeled system of the form

$$\dot{X}_k = \sum_{i=1}^{9} \theta_{ki}\phi_i(X) + \sqrt{\sigma}\dot{W}_k, \quad k = 1, 2, 3, \tag{2.6}$$

where $\phi = \{\phi_i\}$, $i \in \{1, ..., 9\}$ contains all first ($i \in \{1, 2, 3\}$) and second-order ($i \in \{4, .., 9\}$) polynomial basis functions and the W_k are independent $\mathbb{R}$-valued Brownian motions.

In this setting, the modeled system in Eq. (2.6) coincides with the true system in Eq. (2.4) with a proper choice of parameters θ and noise level σ. This example thus serves as a simulation study, while also illustrating the applicability of our sparse discovery method to SDEs, hence going beyond [9].

The parameter vector θ contains 27 unknowns. To ensure well-posedness of the explored model-class, we further impose that the quadratic terms are energy conserving; specifically, we enforce that the inner-product of the quadratic terms with X is identically zero:

$$\sum_{k=1}^{3}\sum_{i=4}^{9} X_k \theta_{ki}\phi_i(X) \equiv 0. \tag{2.7}$$

This ensures that the quadratic term contributes zero energy to the system and is natural from the viewpoint of the geophysical modeling considerations that underpin the model. Mathematically, imposition of (2.7) ensures that the stochastic differential equation does not explode in finite time as it implies boundedness of the second moment at any fixed positive time [52,53]. The constraints in (2.7) number 10, corresponding to removal of X_1^3, X_2^3, X_3^3, $X_1^2 X_2$, $X_1^2 X_3$, $X_2^2 X_1$, $X_2^2 X_3$, $X_3^2 X_1$, $X_3^2 X_2$, and $X_1 X_2 X_3$ from the energy. Consequently, there remain 17 independent unknown coefficients in $\theta = \{\theta_{ki}\}$, $k \in \{1, 2, 3\}$, $i \in \{1, ..., 9\}$ after incorporating the energy constraint. Our goal is to learn a sparse solution θ that has fewer than 17 non-zero elements, as well as the noise level σ. Ideally, in this simulation study, the learnt solution for θ will have 7 non-zero elements that agree with the true system in Eq. (2.4), and a value of σ which agrees with the true value $\sigma^{\dagger}$.

Proposition 1. *Assume that the constraints on parameters $\{\theta_{ki}\}$ are chosen as detailed above, so as to ensure (2.7) holds. Then for any $T > 0$, there are constants $c_1, c_2 > 0$ such that equation (2.6) has, almost surely, a unique solution satisfying $u = (X_1, X_2, X_3) \in C([0, T]; \mathbb{R}^3)$, and*

$$\sup_{t \in [0,T]} \mathbb{E}|u|^2 \leq (|u_0|^2 + c_1)e^{c_2 T}. \quad \diamond$$

Proof. Define the Lyapunov function $V(u) = \frac{1}{2}|u|^2$. Applying the Itô formula to u solving (2.6) gives

$$\frac{d}{dt}\{\mathbb{E}V(u)\} = \mathbb{E}\sum_{k=1}^{3}\sum_{i=1}^{9}X_k\theta_{ki}\phi_i(X) + \sigma.$$

(The precise interpretation of this inequality is in time-integrated form.) Applying (2.7) and noting that the ϕ_i are linear in u for $i = 1, 2, 3$ leads, after application of the Cauchy-Schwarz inequality, to the bound

$$\frac{d}{dt}\{\mathbb{E}V(u)\} \leq \alpha\mathbb{E}V(u) + \sigma$$

for some $\alpha > 0$ (again to be interpreted in integrated form). Integration of the inequality yields the conclusion of the proposition, by application of the moment bound theory of Itô SDEs explained in [52]. $\square$

Example 2.2 (*Lorenz 96 System [54]*). The Lorenz 96 single scale system describes the time evolution of a set of variables $\{x_k\}_{k=1}^{K}$ according to the equations

$$\dot{x}_k = -x_{k-1}(x_{k-2} - x_{k+1}) - x_k + F, \quad k \in \{1, ..., K\},$$
$$x_{k+K} = x_k. \tag{2.8}$$

We choose $K = 36$ and use the system in Eq. (2.8) as the true system for a simulation study. We aim at modeling the unknown tendency with first and second-order polynomial basis functions:

$$\dot{X}_k = \sum_{i=1}^{702}\theta_{ki}\phi_i(X), \quad k = 1, \ldots, 36, \tag{2.9}$$

where $\phi = \{\phi_i\}$, for $i \in \{1, ...702\}$ contains all first ($\phi = \{\phi_i\}$, $| i \in \{1, ..., 36\}$) and second-order polynomial basis functions.

As in Example 2.1, imposition of energy conserving quadratic nonlinearities is important from a modeling point of view and as a means to ensure well-posedness, i.e., existence of solutions to the equation for all time. To this end, we work with a simpler modeled system, from a subclass of the models (2.9), taking the form

$$\dot{X}_k = -X_{k-1}(\beta_k^{(1)}X_{k-2} - \beta_{k+1}^{(1)}X_{k+1}) - (\beta_k^{(2)}X_{k-1}X_k - \beta_{k+1}^{(2)}X_{k+1}^2)$$
$$- (\beta_k^{(3)}X_kX_{k+1} - \beta_{k-1}^{(3)}X_{k-1}^2) - (\beta_k^{(4)}X_{k-1}X_{k+1} - \beta_{k+1}^{(4)}X_{k+1}X_{k+2})$$
$$- \alpha_kX_k + F, \quad k \in \{1, ..., K\}, \tag{2.10}$$
$$X_{k+K} = X_k.$$

Thus, we only introduce the second-order polynomial basis functions that are constructed by a single variable and its two nearest neighbors, together with a linear diagonal term. This incorporates the energy conservation constraint – the inner-product of the quadratic terms with X is identically zero. The boundary conditions for the unknown parameters in Eq. (2.10) are $\beta_{k+K}^{(i)} = \beta_k^{(i)}$ and $\alpha_{k+K} = \alpha_k$ for $i \in \{1, 2, 3, 4\}$ and $k \in \{1, ..., K\}$. Therefore, we have 144 unknowns in β and 36 unknowns in α. Our goal is to learn a sparse solution $\{\{\beta_k^{(i)}\}_{i=1}^{4}, \alpha_k\}_{k=1}^{36}$ which has considerably fewer than 180 non-zero elements. Ideally, of course, in this simulation study setting, the sparse solution will have 72 non-zero elements that agree with the true system in Eq. (2.8).

Proposition 2. *Equation* (2.10) *has unique solution* $u = (X_1, \cdots, X_K) \in C([0, \infty); \mathbb{R}^K)$. $\diamond$

Proof. Define the Lyapunov function $V(u) = \frac{1}{2}|u|^2$. Straightforward computation using (2.10) gives

$$\frac{d}{dt}V(u) \leq \alpha V(u) + \beta$$

for some $\alpha, \beta > 0$ after using the fact that (2.9) holds and using the Cauchy-Schwarz inequality. Integration of the inequality yields the conclusion of the proposition since, for finite dimensional systems, blow-up in finite time is the only way the solution can cease to exist, and the bound precludes this. $\square$

In addition, we also consider a situation in which data are generated by the *multiscale* Lorenz 96 system:

$$\dot{x}_k = -x_{k-1}(x_{k-2} - x_{k+1}) - x_k + F - \frac{hc}{J}\sum_{j=1}^{J} y_{j,k}, \quad k \in \{1, \ldots, K\},$$

$$\frac{1}{c}\dot{y}_{j,k} = -by_{j+1,k}(y_{j+2,k} - y_{j-1,k}) - y_{j,k} + \frac{h}{J}x_k, \quad (j,k) \in \{1, \ldots, J\} \times \{1, \ldots, K\}$$

$$x_{k+K} = x_k, \quad y_{j,k+K} = y_{j,k}, \quad y_{j+J,k} = y_{j,k+1}.$$

(2.11)

We will take the values $K = 36$ and $J = 10$ and work with parameter values in which the X and Y variables are scale-separated. In this setting, the averaging principle enables elimination of the Y variables from the X equation because they are a function of X. Thus, it is natural to try and fit data from the X variable in the multiscale system Eq. (2.11) to a closed equation in X alone, of the form

$$\dot{X}_k = - X_{k-1}(\beta_k^{(1)}X_{k-2} - \beta_{k+1}^{(1)}X_{k+1}) - (\beta_k^{(2)}X_{k-1}X_k - \beta_{k+1}^{(2)}X_{k+1}^2)$$
$$- (\beta_k^{(3)}X_kX_{k+1} - \beta_{k-1}^{(3)}X_{k-1}^2) - (\beta_k^{(4)}X_{k-1}X_{k+1} - \beta_{k+1}^{(4)}X_{k+1}X_{k+2})$$
$$- \alpha_k X_k + F + g(X_k), \quad k \in \{1, ..., K\},$$

$$X_{k+K} = X_k.$$

(2.12)

Comparison with Eq. (2.10) shows that the only difference is an additional function $g(X_k)$. The averaging principle alone does not justify the diagonal and universal form of the closure $g(\cdot)$ but empirical evidence, and arguments based on $J \gg 1$, show that it is a reasonable closure model to employ, an idea developed in [55] and studied further in [29,56]. We use a hierarchical Gaussian process (GP) with 10 unknowns to parameterize the function $g(X_k)$, as introduced in [29]. We learn the GP together with unknown parameters $\{\{\beta_k^{(i)}\}_{i=1}^4, \alpha_k\}_{k=1}^{36}$, based on the data from the multiscale Lorenz 96 system in Eq. (2.11). The sparsity constraint is not put on the GP parameters but only on the $\{\{\beta_k^{(i)}\}_{i=1}^4, \alpha_k\}_{k=1}^{36}$.

Example 2.3 (*Coalescence Equations*). Coagulation and fragmentation equations [57,58] for systems of particles or droplets may be found in the modeling of a wide range of phenomena arising in science and engineering, for example, in cloud microphysics [59,60], or 3D printing [61]. We consider models in which fragmentation does not occur and refer to the resulting process as one of coalescence. The evolution of the coalescence of particles or droplets is described by a transport equation that tracks the evolution of the moments x_k of the mass distribution:

$$\frac{dx_k}{dt} = \frac{1}{2}\int_0^\infty\int_0^\infty \left((m + m')^k - m^k - m'^k\right) \mathcal{C}(m, m')f(m)f(m')\,dm\,dm'.$$

(2.13)

Here, $f(\cdot)$ denotes the mass distribution, and the kernel $\mathcal{C}$ describes the probability of coalescence of two particles or droplets with masses m and m'. We employ the polynomial kernel $\mathcal{C}$ defined via non-negative weights $\{c_{ab}\}$ and the non-negative integer r:

$$\mathcal{C}(m, m') = \sum_{a,b=0}^{r} c_{ab}m^a m'^b.$$

(2.14)

By substituting Eq. (2.14) into the transport equation (2.13), and truncating to consider only moments $k = 1, \cdots, K$, we derive a modeled system to describe the evolution of moments:

$$\frac{dX_k}{dt} = \frac{1}{2}\sum_{a,b=0}^{r}\sum_{j=1}^{k-1}c_{ab}\binom{k}{j}X_{a+j}X_{b+k-j}, \quad k = 2, 3, ..., K,$$

$$\frac{dX_k}{dt} = \begin{cases} -\frac{1}{2}\sum_{a,b=0}^{r}c_{ab}X_aX_b & k = 0, \\ 0 & k = 1. \end{cases}$$

(2.15)

It should be noted that Eq. (2.15) is not a closed system: X_ℓ for $\ell \in \{K+1, ..., K+r-1\}$ are needed in the modeled system. We base the closure model for these higher-order moments on the fitting of a Gamma distribution for $f(\cdot)$. The resulting moment-based coalescence equation with polynomial kernel and Gamma distribution closure is proposed in [62].

Since the mass of the system is X_0, all integrals should be normalized by this number to have the standard probabilistic interpretation. Then, the mean of this probabilistic distribution is X_1/X_0 and the variance is $X_2/X_0 - (X_1/X_0)^2$. If κ and η are the shape and scale parameters of the Gamma distribution, $\kappa\eta$ is the mean and $\kappa\eta^2$ is the variance. This leads to the following Gamma distribution closure, noting that $\Gamma(n) = (n-1)!$:

$$X_k = X_0 \eta^k \frac{\Gamma(\kappa+k)}{\Gamma(\kappa)}, \quad k > K,$$
$$\kappa = \frac{X_1^2}{X_0 X_2 - X_1^2}, \quad \eta = \frac{X_2}{X_1} - \frac{X_1}{X_0}. \tag{2.16}$$

We study the modeled system in Eq. (2.15), (2.16) with $K = 2$ and $r = 3$; thus, we use the closure to determine the variables X_3, X_4 in terms of the primary moments X_0, X_1 and X_2. Our goal in this example is to learn a sparse set of coefficients c_{ab} in Eq. (2.15) based on the data in the following different settings, all using the model in Eq. (2.15) with different parameters and closures for the data generating and fitted models.

- Data are generated and fitted with $K = 2$ and $r = 3$, and with the Gamma distribution closure in Eq. (2.16);
- Data are generated with $K > 2$ and $r = 3$ and fitted with $K = 2$ and $r = 3$, both using the Gamma distribution closure in Eq. (2.16);
- Data are generated with $K = 2$ and $r = 3$ and an exponential closure distribution, and we fit a model for $K = 2$ and $r = 3$ with the Gamma distribution closure in Eq. (2.16).

For the last bullet, we note that the exponential distribution closure has the following form:

$$X_k = X_0 \frac{k!}{\mu^k}, \quad k > 2,$$
$$\mu = \frac{X_0}{X_1}, \tag{2.17}$$

where μ denotes the rate parameter of an exponential distribution, chosen to agree with information present in X_0 and X_1.

To prevent unphysical responses, we constrain the parameters κ and η of the Gamma distribution to prescribed intervals. In so doing, we obtain a closed pair of equations for (X_0, X_2) of the form

$$\dot{X}_0 = -\frac{1}{2} \sum_{a,b=0}^{3} c_{ab} X_a X_b,$$
$$\dot{X}_2 = \sum_{a,b=0}^{3} c_{ab} X_{a+1} X_{b+1}, \tag{2.18}$$

with $X_1(t) \equiv X_1(0)$ and

$$X_k = X_0 \eta^k \frac{\Gamma(\kappa+k)}{\Gamma(\kappa)}, \quad k = 3, 4,$$
$$\kappa' = \frac{X_1^2}{X_0 X_2 - X_1^2},$$
$$\eta' = \frac{X_2}{X_1} - \frac{X_1}{X_0}; \tag{2.19}$$
$$\kappa = \max(\min(\kappa', \kappa_{\max}), \kappa_{\min}),$$
$$\eta = \max(\min(\eta', \eta_{\max}), \eta_{\min}).$$

The moment X_1 is a constant which, throughout the simulations in this paper, is set to be 2. Furthermore we take $\kappa_{\min}$ and $\kappa_{\max}$ to be 10^{-3} and 10, and $\eta_{\min}$ and $\eta_{\max}$ to be 10^{-3} and 1.

Proposition 3. *Let X_0, X_1, X_2 be non-negative at $t = 0$, assume that $c_{11} = 0$ and that $c_{ab} \geq 0$ for $0 \leq a, b \leq 4$ and that $0 < \kappa_{\min} < \kappa_{\max} < \infty$, $0 < \eta_{\min} < \eta_{\max} < \infty$. Let $T \in (0, \infty]$ be the first time at which X_0 or X_2 becomes zero. Then, the equations (2.18) and (2.19) for $u = (X_0, X_2)$ have a unique solution $u \in C^1([0, T]; \mathbb{R}^2)$.* ◇

Proof. Recall that X_1 is constant in time. We consider solutions only in the time-interval $[0, T]$. The imposed upper and lower bounds on κ and η ensure that the closure model has the property that there is a universal constant $\mathsf{c} \in (0, 1)$ such that, while a solution to the equations for X_0, X_2 exists (and necessarily remains non-negative) in $[0, T]$,

$$\mathsf{c} X_0 \leq X_3 \leq \mathsf{c}^{-1} X_0, \quad \mathsf{c} X_0 \leq X_4 \leq \mathsf{c}^{-1} X_0.$$

It follows from the equation for X_0 that, for $t \in [0, T]$,

$$0 \leq X_0(t) \leq X_0(0)$$

since all quantities on the right hand-side of the equation for $\dot{X}_0$ in (2.18) are negative. Now note that the right hand side of the equation for $\dot{X}_2$ in (2.18) contains no quadratic terms in X_2, since $c_{11} = 0$, and that the constant term and linear coefficient (with respect to X_2) on the right hand side are, for $t \in [0, T]$, bounded. Multiplying the equation by X_2 shows that $V(X_2) = |X_2|^2$ satisfies

$$\frac{d}{dt} V(X_2) \leq \alpha + \beta V(X_2)$$

with α, β determined by the initial conditions and c. Hence X_2 cannot blow-up in $[0, T]$ and the result is proved. $\qquad\square$

The total number of unknowns to be learned is 9, after imposing symmetry on c_{ab} and setting c_{11} to zero. We also have a positivity constraint on all unknowns. Adding a constraint $c_{22} = 0$ can be used to prevent X_0 from becoming negative, thereby extending the preceding proposition to hold for all $t \geq 0$. In practice, however, we find that the sparse solution always enforces $c_{22} = 0$ and that we do not need to impose it.

Example 2.4 (*Kuramoto-Sivashinsky Equation*). Let $\mathbb{T}^L$ denote the torus $[0, L]$ and consider the equation

$$\partial_t u = -\partial_x^4 u - \partial_x^2 u - u \partial_x u, \quad x \in \mathbb{T}^L,$$

$$u|_{t=0} = u_0.$$

(2.20)

We are interested in learning this model from a library of equations of the form

$$\partial_t u = -\sum_{j=1}^{5} \left(\alpha_j \partial_x^j u + \beta_j u^j \partial_x u \right), \quad x \in \mathbb{T}^L,$$

$$u|_{t=0} = u_0.$$

(2.21)

Thus, we have 10 unknowns. We wish to constrain the model so that solutions do not blow up in finite time. To do this, we ensure that $\|u\|_{L^2(\mathbb{T};\mathbb{R})}$ remains bounded. Note that the nonlinear terms disappear when multiplied by u and integrated over $\mathbb{T}^L$, because of periodicity. On the other hand, the linear term will damp all high spatial frequencies, uniformly in sufficiently large wave-number, provided that $\alpha_4 > 0$. Thus we have:

Proposition 4. *Let $\alpha_4 > 0$. Then there is constant c > 0 such that the solution of equation* (2.21)*, if it exists as a function $u \in C([0, T]; L^2(\mathbb{T}; \mathbb{R}))$, satisfies*

$$\sup_{t \in [0,T]} \|u\|_{L^2(\mathbb{T};\mathbb{R})}^2 \leq \|u_0\|_{L^2(\mathbb{T};\mathbb{R})}^2 e^{cT}. \quad \diamond$$

Proof. Let

$$V(u) = \frac{1}{2} \|u\|_{L^2(\mathbb{T};\mathbb{R})}^2.$$

Using periodicity we note that

$$\int_{\mathbb{T}} u \times \beta_j u^j \partial_x u \, dx = 0$$

and that, for j odd,

$$\int_{\mathbb{T}} u \times \alpha_j \partial_x^j u \, dx = 0.$$

Thus we obtain, provided a solution exists,

$$\frac{d}{dt} V(u) \leq -\alpha_2 \int_{\mathbb{T}} u \times \partial_x^2 u \, dx - \alpha_4 \int_{\mathbb{T}} u \times \partial_x^4 u \, dx.$$

A straightforward calculation based on the spectrum of the operator L defined by $Lu := \alpha_2 \partial_x^2 u + \alpha_4 \partial_x^4 u$ on $\mathbb{T}$ shows that there is constant c > 0 such that

$$\frac{d}{dt}V(u) = -\int_{\mathbb{T}} u \times Lu\, dx \leq \mathsf{c}V(u),$$

and the proof is complete. □

In summary we have 10 unknowns, and a positivity constraint on one of the unknowns. Although we ensure that the ℓ_2-norm of the simulated state remains bounded, it is still possible that the simulated state may blow-up due to numerical discretization. Therefore, we also implement numerical clipping to bound the simulated state at every time step. Details concerning the numerical solution of the K-S equation, including the clipping used, are presented in Appendix A.

3. Algorithms

Let $G_\tau(\theta; x_0)$ denote the data found by time-averaging a trajectory started from x_0 over time duration τ. The initial condition x_0 is not known to us and is not of intrinsic interest. Thus, we view the given data, $y \in \mathbb{R}^J$, as a noisy evaluation of the ergodic ($\tau = \infty$) average $\mathcal{G}(\theta)$ in which the dependence on x_0 disappears. Appealing to central limit theorem results that quantify rates of convergence towards ergodic averages [63], we may formulate the inverse problem as follows: given $y \in \mathbb{R}^J$, find $\theta \in \Theta$ so that

$$y = G_\tau(\theta; x_0) \approx \mathcal{G}(\theta) + \eta, \quad \eta \sim N\big(0, \Gamma(\theta)\big). \tag{3.1}$$

In practice we make the approximation that Γ is constant with respect to parameter θ and we solve the resulting Bayesian inverse problem

$$y = \mathcal{G}(\theta) + \eta, \quad \eta \sim N\big(0, \Gamma\big). \tag{3.2}$$

The noise variance Γ is estimated using timeseries of different lengths; see [64] for details. We also note that $\mathcal{G}(\theta)$ is not computable and only available to us through noisy approximate evaluations. The natural objective function associated with the inverse problem (3.2) is

$$\frac{1}{2}\big|\Gamma^{-\frac{1}{2}}\big(y - \mathcal{G}(\theta)\big)\big|^2. \tag{3.3}$$

We study the use of EKI based methods for solving this inverse problem. The four primary reasons for using EKI to solve the inverse problem are: (a) EKI does not require derivatives, which are difficult to compute in this setting of SDEs; nonetheless, EKI provably, in the linear case [37,39], and approximately, in the nonlinear case [65] behaves like a gradient descent with respect to objective (3.3), projected into a finite dimensional space defined by the ensemble; (b) EKI is robust to noisy, approximate evaluations of the forward map as shown in [66]. (c) EKI is inherently parallelizable and scales well to high-dimensional unknowns [32,67]. (d) EKI lends itself naturally to the imposition of constraints on the unknown parameters [42]. The primary novelty of the approach proposed in this paper is the demonstration that imposition of sparsity within EKI is something that can be achieved easily and that enables generalization of the approach pioneered in [9] to settings in which the observations are nonlinear and partial and in which the dynamical system comes from an SDE. Such problems lead to the parameter learning of θ from data y related by inversion of (3.2).

In subsection 3.1, we recap the basic EKI algorithm to fit unknown parameters. In particular, we demonstrate how the iterative algorithm, which is nonlinear, has at its core a quadratic optimization problem. In subsection 3.2, we describe a method of inducing sparsity within the EKI algorithm, by introducing an ℓ_1 constraint and/or an ℓ_0 penalty on top of the core optimization task solved by the basic EKI algorithm. In subsection 3.3, we describe how we reformulate the sparsity inducing step of the algorithm as a standard quadratic programming problem.

There are many variants on the precise manner in which sparsity constraints are imposed, and the algorithms used to solve the resulting optimization problems. Our purpose is not to determine the best way to impose sparsity or to the best way to solve the optimization problems: these are well-studied problems and we simply employ some successful approaches to their resolution. Rather, our purpose is to demonstrate that the EKI approach to parameter learning is easily extended to incorporate sparsity constraints because at its core is solution of a quadratic optimization problem.

3.1. Ensemble Kalman inversion

The EKI algorithm we employ to solve the inverse problem in (3.2) is described in [38,42]. First, we introduce a new variable $w = \mathcal{G}(\theta)$ and variables v and $\Psi(v)$:

$$\begin{aligned} v &= (\theta, w)^\top, \\ \Psi(v) &= (\theta, \mathcal{G}(\theta))^\top. \end{aligned} \tag{3.4}$$

Using these variables, we formulate the following noisily observed dynamical system:

$$v_{m+1} = \Psi(v_m)$$
$$y_{m+1} = H v_{m+1} + \eta_{m+1}. \tag{3.5}$$

Here, $H = [0, I]$, $H^\perp = [I, 0]$, and hence $Hv = w$ and $H^\perp v = \theta$. In this setting, $\{v_m\}$ is the state and $\{y_m\}$ are the data. The objective is to estimate $H^\perp v_m = \theta_m$ from $\{y_\ell\}_{\ell=1}^m$ and to do so iteratively with respect to m. In practice, we only have one data point y and not a sequence y_m, and we only have noisy approximations of $\mathcal{G}(\theta)$. We thus introduce noisy, computable, perturbations $y_m^{(j)}$, $G_m^{(j)}$ and $\Psi_m^{(j)}$ of the data y and maps , $\mathcal{G}$, Ψ; details are given after presenting the algorithm in its basic form.

The EKI algorithm creates an ensemble $\{v_m^{(j)}\}_{j=1}^J$ defined iteratively in m as follows:

$$J_m^{(j)}(v) := \frac{1}{2}\left|y_{m+1}^{(j)} - Hv\right|_\Gamma^2 + \frac{1}{2}\left|v - \Psi_m^{(j)}\left(v_m^{(j)}\right)\right|_{C_m^{\Psi\Psi}}^2,$$
$$v_{m+1}^{(j)} = \arg\min_v J_m^{(j)}(v). \tag{3.6}$$

The matrix $C^{\Psi\Psi}$ is the empirical covariance of $\{\Psi_m^{(j)}(v_m^{(j)})\}_{j=1}^J$. At each step m, J ensemble parameter estimates indexed by $j = 1, \cdots, J$ are found from $\theta_m^{(j)} = H^\perp v_m^{(j)}$.

Using the fact that $v = (\theta, w)^T$, the minimizer $v_{m+1}^{(j)}$ in (3.6) decouples to give the update formula

$$\theta_{m+1}^{(j)} = \theta_m^{(j)} + C_m^{\theta G}\left(C_m^{GG} + \Gamma\right)^{-1}\left(y_{m+1}^{(j)} - G_m^{(j)}(\theta_m^{(j)})\right); \tag{3.7}$$

the matrix C_m^{GG} is the empirical covariance of $\{G_m^{(j)}(\theta_m^{(j)})\}_{j=1}^J$, while the matrix $C_m^{\theta G}$ is the empirical cross-covariance of $\{\theta_m^{(j)}\}_{j=1}^J$ with $\{G_m^{(j)}(\theta_m^{(j)})\}_{j=1}^J$. Details of the derivation may be found in [38,42]. The algorithm preserves the linear span of the initial ensemble $\{\theta_0^{(j)}\}_{j=1}^J$ for each m and thus operates in a finite-dimensional vector space, even if Θ is an infinite-dimensional vector space.

The data $y_{m+1}^{(j)}$ are either fixed, so that $y_{m+1}^{(j)} \equiv y$, or created by adding random draws to y from the distribution of η, independently for all m and j; this extra noise has potential benefits analogous to the use of stochastic gradient descent [8]. We now detail exactly how $y_m^{(j)}$ and $G_m^{(j)}(\cdot)$ are defined; from the latter we define $\Psi_m^{(j)}(\theta) = (\theta, G_m^{(j)}(\theta))^T$. In the experiments reported in this paper, we add i.i.d. (w.r.t. j and m) random mean zero Gaussian noise with covariance Γ to the data y to obtain $y_m^{(j)}$; however, we have verified that near identical parameter estimates are obtained in the same number of iterations without adding any random noise to y, for several of the experiments reported. The noisy approximate forward model is defined by $G_m^{(j)}(\cdot) = G_T(\cdot; x_0^{(j,m)})$. The initial condition $x_0^{(j,m)}$ is chosen at random, i.i.d. with respect to both ensemble member j and iteration step m, except for the examples of coalescence equations that use fixed initial conditions. Details are given for each example in what follows. Note that the finite time T in $G_m^{(j)}$ is typically different from τ arising in the time-averaged data.

3.2. Sparse ensemble Kalman inversion (EKI)

We are interested in finding a sparse solution θ of the inverse problem in (3.2), building on the key features (a)–(d) possessed by EKI and outlined in the preamble to this section. To impose sparsity on the solution of θ from EKI, we replace the step (3.6) with the step

$$J_m^{(j)}(v, \lambda) := \frac{1}{2}\left|y_{m+1}^{(j)} - Hv\right|_\Gamma^2 + \frac{1}{2}\left|v - \Psi_m^{(j)}\left(v_m^{(j)}\right)\right|_{C_m^{\Psi\Psi}}^2 + \lambda|H^\perp v|_{\ell_0},$$
$$v_{m+1}^{(j)} = \arg\min_{v \in \mathfrak{V}} J_m^{(j)}(v), \tag{3.8}$$

where

$$\mathfrak{V} = \{v : |H^\perp v|_{\ell_1} \le \gamma\}. \tag{3.9}$$

On occasion we will also impose positivity constraints on some of the parameters and will then choose, for some matrix A,

$$\mathfrak{V} = \{v : |H^\perp v|_{\ell_1} \le \gamma, \; AH^\perp v \ge 0\}. \tag{3.10}$$

The parameters γ and λ may be adjusted and indeed could be learned via cross-validation. To solve the resulting optimization problem, we alternate minimization of (3.8) for $\lambda = 0$, which approximates a gradient descent step for (3.3) subject to an ℓ_1 constraint, with a proximal gradient step on the $|\cdot|_{\ell_0}$ norm, projected into the ℓ_1 constraint set; however, the latter cannot leave either of the constraint sets (3.9) or (3.10), and so reduces to a simple λ-dependent thresholding. To this end, we introduce the function $\mathcal{T}$ on vectors defined by

$$\mathcal{T}(\theta_i) = \begin{cases} 0, & \text{if } |\theta_i| < \sqrt{2\lambda} \\ \theta_i, & \text{otherwise.} \end{cases} \tag{3.11}$$

With this definition, we arrive at Algorithm 1.

Algorithm 1 Sparse EKI algorithm.

1: Choose $\{\theta_m^{(j)}\}_{j=1}^J$ for $m = 0$
2: $\{w_m^{(j)} = G_m^{(j)}(\theta_m^{(j)})\}_{j=1}^J$
3: **for** $j = 1, 2, ..., J$ **do**
4:     $v_{m+1}^{(j)} \leftarrow$ argmin of (3.8) with $\lambda = 0$
5:     Extract $\theta_{m+1}^{(j)} = H^\perp v_{m+1}^{(j)}$
6:     $\theta_{m+1}^{(j)} = \mathcal{T}(\theta_{m+1}^{(j)})$
7: **end for**
8: $m \leftarrow m + 1$, go to 2

Remark 3.1. The quadratic programming problem solved at each step m in this algorithm only incorporates the ℓ_1 constraint; thresholding, to enforce the ℓ_0 constraint, is performed after solving the quadratic programing problem. Note that $\lambda = 0$ in step 4 of Algorithm 1. Thus the standard EKI update (3.7) may be applied in step 4, and the resulting output employed, if the constraints are satisfied by the output; when they are not satisfied, the optimization problem (3.8) must be solved. Taking $\lambda = 0$ results in a modification of EKI that promotes smaller ℓ_1-norm solutions; the subsequent λ-dependent thresholding in step 6 enforces the sparsity suggested by the smaller ℓ_1-norm solution and induces a smaller ℓ_0 norm. In the next subsection, we give details about how to formulate the optimization problem Eq. (3.8) with $\lambda = 0$ as a standard quadratic programming problem, rendering the preceding algorithm not only implementable, but efficient.

Remark 3.2. In the case $\gamma = \infty$ and $\lambda = 0$, the algorithm reduces to alternation of standard EKI (which behaves like a step of gradient descent) with a hard-thresholding algorithm. This can lead to solutions that reach ensemble consensus (we refer to this as collapse) at incorrect parameter values. To avoid this, Algorithm 1 is formulated with $\gamma < \infty$ and $\lambda = 0$. We find that including both the ℓ_1-constraint and hard-thresholding in this manner provides a more effective algorithm.

Remark 3.3. Both Γ and $C_m^{\Psi\Psi}$ in (3.8) are independent of the ensemble index j, and thus Algorithm 1 is parallelizable.

In practice, the coefficients $\theta^{(j)}$ identified by a single sparsity-promoting optimization, such as Algorithm 1, will exhibit bias. To enhance the performance of identifying the coefficients $\theta^{(j)}$, it is sometimes useful to run the sparse EKI Algorithm 1 in multiple batches, removing unnecessary basis functions in each batch, until the number of basis functions cannot be further reduced. Similar concepts, employing multiple optimizations sequentially, are also advocated in [9,12]. More specifically, iteratively thresholded least squares optimization is recommended in [9], that is, iteratively solving the least squares optimization on reduced basis functions identified by the optimization in the previous step. On the other hand, a second least squares optimization restricted to the features identified from the original ℓ_1 penalized least squares optimization is recommended in [12]. There is also theoretical work related to debiasing the output of sparse solution algorithms; see [68]. However our approach is more closely linked to the ad hoc approaches advocated in [9,12].

3.3. Quadratic programming with ℓ_1 penalty

The objective function in (3.8) with $\lambda = 0$ can be rewritten (neglecting constants in v) as, for $C_m = C_m^{\Psi\Psi}$,

$$\frac{1}{2} v^\top \left(H^\top \Gamma^{-1} H + C_m^{-1} \right) v - \left(C_m^{-1} \Psi(v_m^{(j)}) + H^\top \Gamma^{-1} y^{(j)} \right)^\top v. \tag{3.12}$$

We wish to minimize over $\mathfrak{V}$ defined in (3.10) (the case (3.9) may be extracted from what follows simply by setting $A = 0$). By appropriate definition of Q and q, we may write the resulting minimization problem as

$$\begin{aligned} \min_v \quad & \frac{1}{2} v^\top Q v + q^\top v \\ \text{s.t.} \quad & A H^\perp v \geq 0, \ \left| H^\perp v \right|_{\ell_1} \leq \gamma. \end{aligned} \tag{3.13}$$

The following decomposition as described in [6] can be employed to convert (3.13) into the standard form of quadratic programming: introduce variables

$$\begin{aligned} v_i &= v_i^+ - v_i^-, \\ |v_i| &= v_i^+ + v_i^-, \end{aligned} \tag{3.14}$$

where $v_i^+ \geq 0$ and $v_i^- \geq 0$ denote the positive and negative part of the ith element of v, respectively. This decomposition leads to the following minimization problem:

$$
\min_{v^+, v^-} \quad \frac{1}{2} \left(v^+ - v^- \right)^\top Q \left(v^+ - v^- \right) + q^\top \left(v^+ - v^- \right)
$$
$$
\text{s.t.} \quad A H^\perp \left(v^+ - v^- \right) \geq a, \; H^\perp \left(v^+ + v^- \right) \leq \gamma, \; v^+ \geq 0, \; v^- \geq 0.
$$

(3.15)

If we define the augmented vector $u^\top = \left[v^+, v^- \right] \in \mathbb{R}^{2z}$, we see that the problem takes the form of a standard quadratic programming problem; alternatively one may work with the variable $u^\top = \left[\left(v^+ - v^- \right)^\top, \left(v^+ + v^- \right)^\top \right] \in \mathbb{R}^{2z}$.

Remark 3.4. The quadratic programming problem arising here by application of the approach pioneered in [6] is a classic problem; we solve it using a state-of-the-art package [69]. In addition to the approach we adopt to imposing sparsity, there are other methods that solve convex optimization problems such as (3.8) subject to ℓ_1 regularization or penalty. These include the alternating direction method of multipliers (ADMM) [70] and split Bregman method [71]. Our formulation of the problem in (3.8) as a standard quadratic programming problem has the benefit that other equality and/or inequality constraints are readily imposed on the EKI methodology, along with the ℓ_1 regularization of penalization, as explained in [42].

Remark 3.5. In some applications, it may be of interest to impose sparsity only on a subset of the parameters θ. The modification required to do this is straightforward and so we do not detail it here. Such a modification is employed in the next section when we learn a closure model for the Lorenz 96 multiscale equations.

Remark 3.6. Numerical issues arising in solution of the quadratic program can be triggered by ensemble collapse as the empirical covariance $C_m^{\Psi,\Psi}$ then becomes close to singular; both the EKI iteration itself, or the thresholding, can exacerbate this issue. This can be ameliorated by use of a small covariance inflation. In practice, throughout this paper, we add a centered normal covariance matrix (zero mean and standard deviation of 10^{-3}) to $C_m^{\Psi,\Psi}$ to avoid such numerical issues.

Remark 3.7. The numerical examples in this work were conducted with ensemble sizes greater than the number of unknown parameters. To deal with the opposite situation, the operator splitting algorithm in [12] may be used. This approach introduces desirable regularization within a standard quadratic programming problem and is useful in the presence of numerical issues such as those caused by low-rank covariance matrices based on a relatively small ensemble size. However, the sampling error for small ensemble sizes can still impact the performance of standard EKI updates. To address this issue, [72] introduces a sampling error correction by constructing a multiplicative correction function via an offline Monte-Carlo computation. Similar ideas were also studied by [73] in the context of ensemble Kalman filters, where localization of covariances is used to address sampling noise from small ensemble sizes for problems without a well-defined distance function between parameters. Introducing localization can also help overcome the limitation of restricting the solution to the subspace spanned by the initial ensemble [74]; the explicit convex optimization step used in this work achieves a similar effect.

4. Numerical results

We demonstrate the capability of the proposed methodology by studying the four examples introduced in Section 2. In all cases, the unknown parameters are detailed in Section 2 and the data used to learn them are detailed in what follows. For the noisy Lorenz 63 system, we use the Euler-Maruyama method to solve the Itô SDEs. For the Lorenz 96 systems, we use an adaptive numerical integrator [75,76] that automatically chooses between the nonstiff Adams method and the stiff BDF method. For the coalescence equation, we use the fourth-order Runge–Kutta method. The numerical integrator for the Kuramoto-Sivashinsky equation is presented in Appendix A. In all cases, the results are initially presented in two figures, one showing the ability of the sparse EKI method to fit the data, and a second showing that the proposed methodology indeed provides a sparse solution in terms of the ℓ_1 norm of redundant coefficients. The results show that the proposed sparse EKI method is capable of fitting the data well and correctly captures the sparsity of the true system. For the chaotic problems, we study how the fitted dynamical system performs in terms of reproducing the invariant measure and time correlation of the true system. To make this comparison, the true invariant measure and autocorrelation are computed from ensemble simulations over a long time interval (in the case of the autocorrelations using a single simulation); the long-time is chosen to ensure that the effect of initialization is negligible. The results comprising predicted and true invariant measures and autocorrelation functions demonstrate that the fitted model using our sparse EKI method can generalize beyond the training data. For the coalescence equation, we evaluate the fitted dynamical system by looking at its ability to reproduce time trajectories of states with a different initial condition from that generating the training data. For the Kuramoto-Sivashinsky equation, we present the results of an additional sparse EKI on a reduced set of basis functions identified by a first, preliminary run of the sparse EKI. All numerical studies confirm that the sparsity-promoting EKI is able to discover the governing equations of dynamical systems based on statistics derived from time series averages.
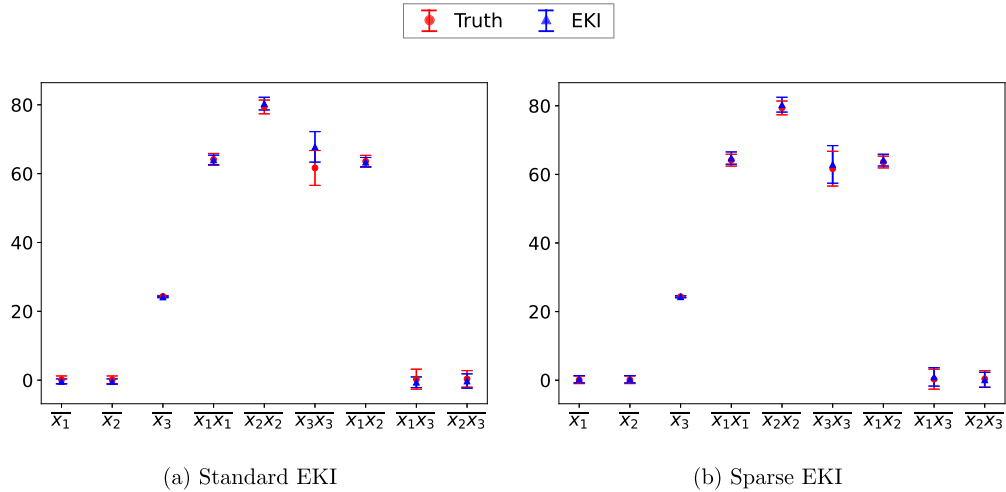
(a) Standard EKI   (b) Sparse EKI

Fig. 1. First two moments of state X for noisy Lorenz 63 system found by using (a) standard EKI and (b) sparse EKI.

Table 1
Mean value of coefficients estimated by standard EKI for all redundant terms.

	Redundant terms					
Equation X_1	X_3	$X_2 X_2$	$X_3 X_3$	$X_1 X_2$	$X_1 X_3$	$X_2 X_3$
Coefficient	-0.229	0.026	0.011	-0.062	-0.093	0.094
Equation X_2	X_3	$X_1 X_1$	$X_3 X_3$	$X_1 X_2$	$X_2 X_3$	
Coefficient	0.099	0.062	-0.008	-0.026	-0.001	
Equation X_3	X_1	X_2	$X_1 X_1$	$X_2 X_2$	$X_1 X_3$	$X_2 X_3$
Coefficient	-0.107	-0.066	0.093	0.001	-0.011	0.008

Throughout our numerical studies, the ensemble size is chosen as 100, unless specified otherwise. The noise Γ is estimated based on the ensemble of time-averaged data from the system with random initial conditions. The averaging time for estimating Γ is the same as the one that we use to gather time-averaged statistics, and the detailed values are described in each example.

4.1. Lorenz 63 system

We first study a noisy Lorenz 63 system for which the data are obtained by simulating (2.4), with a given set of parameters $\alpha = 10$, $\rho = 28$, $\beta = 8/3$, and $\sigma = 10$. The goal is to fit a modeled system (2.6) by learning unknown coefficients θ_{ki} and σ. In this study, $\phi = \{\phi_i\}$, $i \in \{1, ..., 9\}$ contains all the first ($i \in \{1, 2, 3\}$) and second-order polynomial basis functions. It is well known that the existing sparsity-promoting model discovery frameworks such as SINDy [9] would encounter some difficulties for such a system due to noise in the time trajectories. We show that the sparse EKI is able to learn a noisy chaotic system based on statistics derived from averaging time series. Results are presented in Figs. 1 to 4.

The data in this case are finite-time averaged approximations of first and second moments of simulated states. The time-interval used to gather time-averaged statistics is $T = 100$. Therefore, we are learning 18 unknown coefficients (17 independent coefficients in $\{\theta_{ki}\}$ and a constant σ), using a data vector y of dimension 9, as shown in Fig. 1. The initial ensemble of unknown coefficients θ_{ki}, corresponding to the parameters α, ρ and β, are uniformly drawn from $[8, 12]$, $[25, 30]$ and $[2, 4]$. The initial ensemble of the redundant coefficients are uniformly drawn from $[-1, 1]$. The initial ensemble of σ is uniformly drawn from $[0.1, 15]$. The initial condition $x_0^{(j,m)}$ is uniformly drawn from $[0, 1]$. We use 50 EKI iterations. The sparsity promoting parameters γ (appearing in the optimization step) and $\sqrt{2\lambda}$ (appearing in the thresholding step) are chosen as 60 and 0.1. The comparison between the true data and the results of the estimated systems in Fig. 1 shows that the sparse EKI has slightly better agreement with the true data than does standard EKI.

The ℓ_1-norm of all redundant coefficients also demonstrates the improved performance using sparse EKI, as presented in Fig. 2. Compared to the results of standard EKI, the ℓ_1-norm of all redundant coefficients is driven much closer to zero using sparse EKI. The coefficients of redundant terms estimated by standard EKI are presented in Table 1, where we can see that there are a few terms being identified with coefficients noticeably larger than zero, such as the linear term X_3 in the equation for X_1. On the other hand, sparse EKI drives all coefficients of the redundant terms close to zero as shown by Fig. 2b.

We further investigate the performance of the estimated systems by evaluating the invariant measure. As presented in Fig. 3, the results of sparse EKI show better agreement with the true invariant measure for all three states, confirming
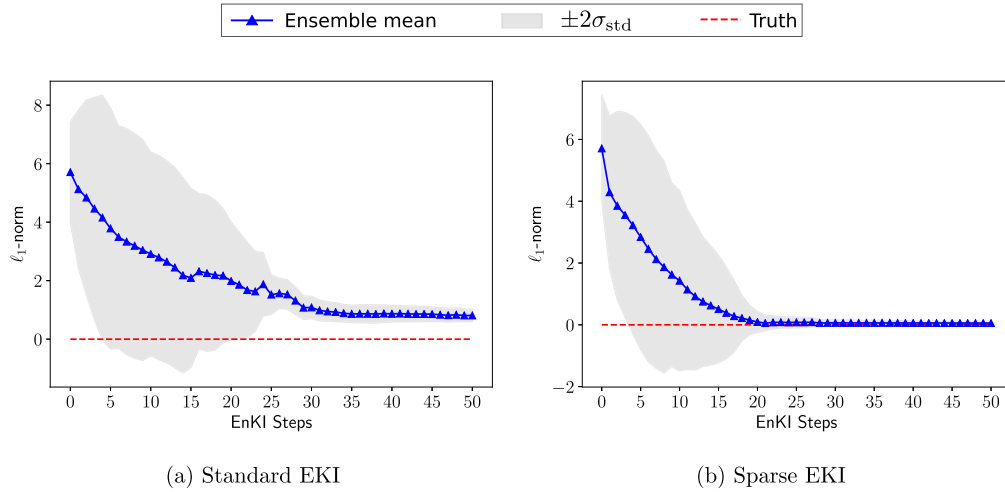
(a) Standard EKI   (b) Sparse EKI

Fig. 2. ℓ_1-norm of redundant coefficients for noisy Lorenz 63 system found by using (a) standard EKI and (b) sparse EKI.
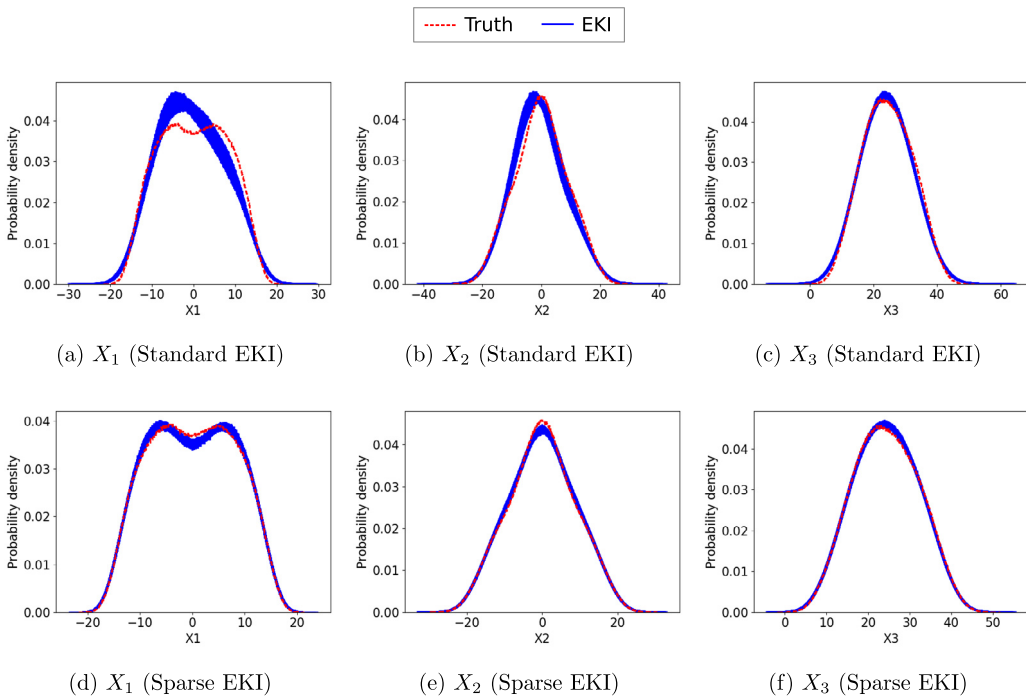

(a) X_1 (Standard EKI)   (b) X_2 (Standard EKI)   (c) X_3 (Standard EKI)

(d) X_1 (Sparse EKI)   (e) X_2 (Sparse EKI)   (f) X_3 (Sparse EKI)

Fig. 3. Invariant measure for noisy Lorenz 63 system found by using (a-c) standard EKI and (d-f) sparse EKI.

the improved performance of the sparse EKI-estimated system over that found from standard EKI, in the long-time limit. The comparison of autocorrelation functions is presented in Fig. 4, demonstrating a good agreement of both EKI estimated systems with the true system in terms of time correlation. When comparing results in Fig. 4, the time correlation results of sparse EKI show slightly better performance than the ones of standard EKI, especially for the simulated states X_1.

Remark 4.1. For this example, we studied in detail the choice of the ℓ_1 penalty parameter γ arising in (3.13) and the thresholding parameter λ in (3.11). As presented in Fig. 5a, smaller γ tends to provide smaller $|\theta|_{\ell_1}$, which indicates a simpler model. The data mismatch dramatically increases when γ is less than around $\gamma = 50$, demonstrating underfitting. On the other hand, both data mismatch and model complexity increase slowly for $\gamma \geq 60$, showing that the performance of the proposed method is not sensitive to the choice of γ provided it is sufficiently large. The comparison of results using different thresholding parameter λ in Fig. 5b shows that the performance of the proposed method is not sensitive to λ. In the example of the noisy Lorenz 63 system, we choose $\gamma = 60$ and $\sqrt{2\lambda} = 0.1$, based on these observations. Since the
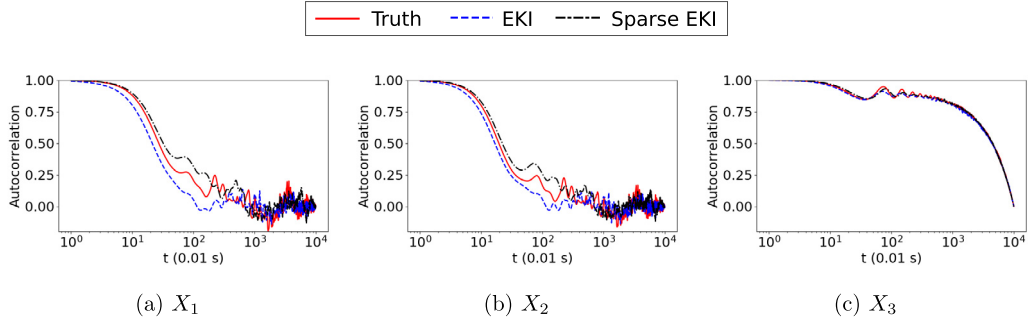
Fig. 4. Autocorrelation for noisy Lorenz 63 system found by using standard EKI and sparse EKI.

(a) ℓ_1 penalty coefficient

(b) Thresholding parameter
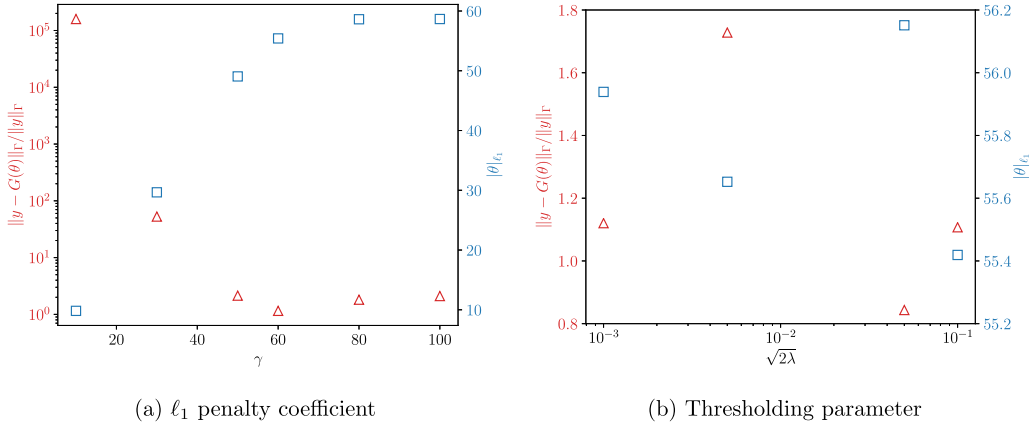
Fig. 5. Parametric study of (a) ℓ_1 penalty coefficient γ and (b) thresholding parameter λ. The data mismatch (left axis) is denoted by triangles ($\triangle$), and the model complexity (right axis) is denoted by squares ($\square$).

proposed method is not sensitive to γ or λ outside the underfitting regime, the parametric study is not presented in other examples for simplicity. It would, of course, be useful to automate the choice of γ and λ via cross-validation.

4.2. Lorenz 96 system

In this subsection, we study two examples of the Lorenz 96 system: (1) a simulation study for which the true and modeled systems are both single-scale Lorenz 96 systems; (2) a more realistic study for which the true system is a multi-scale Lorenz 96 system and the modeled system only resolves the slow variables. In both examples, the sparsity promoting parameters γ (optimization) and $\sqrt{2\lambda}$ (thresholding) are chosen as 72 and 0.1. The initial condition $x_0^{(j,m)}$ is uniformly drawn from $[-5, 10]$.

4.2.1. Simulation study

For this simulation study, the data are generated from the single-scale Lorenz 96 system in (2.8). The goal is to fit a model as shown in (2.10) by using sparse EKI. Therefore, we are fitting 180 unknown coefficients in total, as denoted by $\{\{\beta_k^{(i)}\}_{i=1}^4, \alpha_k\}_{k=1}^{36}$, using a data vector y of dimension 44 (only observing the finite-time average approximation of first and second moments $\{\{\mathcal{G}_1(X), \mathcal{G}_2(X)\}$ for the first 8 state variables). The duration used for time-averaging is $T = 100$. In this case, we use an ensemble size of 400. The initial ensemble of unknown coefficients is uniformly drawn from $[0.7, 1.3]$. We use 10 EKI iterations. Results are presented in Figs. 6 to 9.

The comparison of EKI results with data from the true system is presented in Fig. 6. This shows that the results of both standard EKI and sparse EKI have good agreement with the true system in data space. However, the ℓ_1-norm of redundant coefficients presented in Fig. 7 indicates that some redundant coefficients are not close to zero for the system identified by the standard EKI, while most redundant coefficients are driven to zero using sparse EKI.

The long-time limit performance is investigated by evaluating the invariant measure, as presented in Fig. 8. We can see that both systems identified by standard EKI and sparse EKI show a good agreement with the invariant measure of the true system, while there is slightly greater uncertainty in the invariant measures of the ensemble simulations from standard EKI. As for the invariant measures, the comparison of autocorrelation functions presented in Fig. 9 shows similar performance of
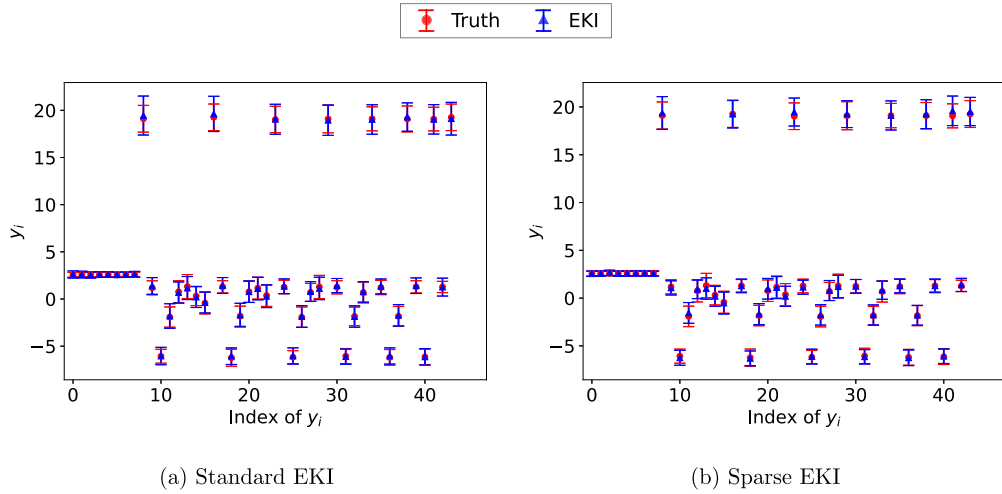
(a) Standard EKI   (b) Sparse EKI

Fig. 6. First two moments of state X for single-scale Lorenz 96 system found by using (a) standard EKI and (b) sparse EKI.

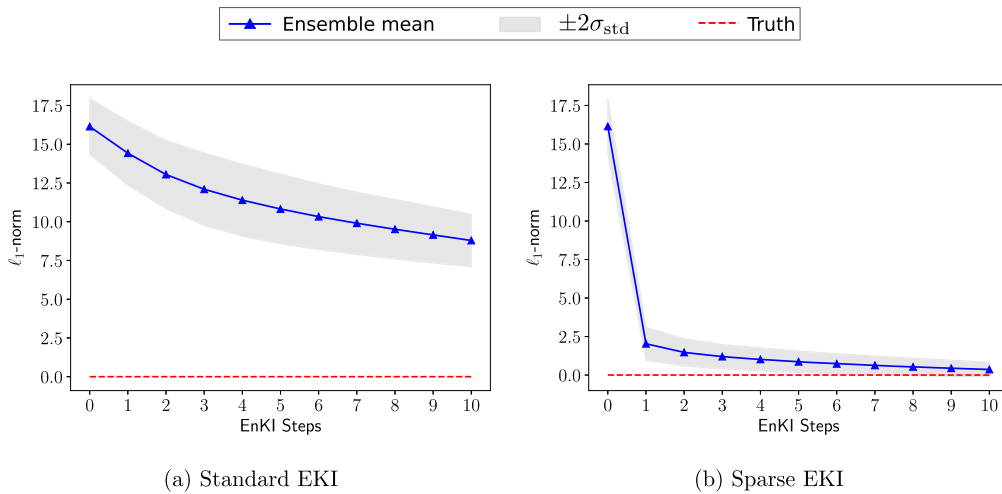(a) Standard EKI   (b) Sparse EKI

Fig. 7. ℓ_1-norm of redundant coefficients for single-scale Lorenz 96 system found by using (a) standard EKI and (b) sparse EKI.

the systems identified by standard EKI and sparse EKI, and both systems have good agreement with the autocorrelation of the true system.

4.2.2. Multi-scale data

We now study a more realistic problem for which the data are generated from the multi-scale Lorenz 96 system in (2.11), and the goal is to fit a reduced-order model as shown in (2.12) by using sparse EKI. Therefore, we are fitting 190 unknown coefficients (180 coefficients as denoted by $\{\{\beta_k^{(i)}\}_{i=1}^{4}, \alpha_k\}_{k=1}^{36}$ and 10 coefficients of GP), using a data vector y of dimension 44 (only observing the finite-time average approximation of first and second moments for the first 8 state variables). The time for gathering averaged statistics is $T = 100$. In this case, we use an ensemble size of 400. The initial ensemble of unknown coefficients $\beta_k^{(i)}$ and α_k are drawn uniformly from $[0.7, 1.3]$. The initial ensemble for the GP mean is defined by parameters drawn uniformly from $[-1, 1]$ at seven points uniformly distributed within $[-15, 15]$. The initial ensemble of the GP observation error is uniformly drawn from $[0.1, 1]$. The initial ensemble of the GP standard deviation and length scale are uniformly drawn from $[0.1, 1]$ and $[5, 20]$. We use 10 EKI iterations. Results are presented in Figs. 10 to 13.

We first present the moments from the system estimated by EKI results and from the true system in Fig. 10. Although the results of standard EKI show relatively good agreement with the true data in Fig. 10a, the results of sparse EKI demonstrate a better agreement with true data in Fig. 10b. The better performance of sparse EKI is also confirmed by the comparison of the ℓ_1-norm of all redundant coefficients presented in Fig. 11. The comparison in Fig. 11 indicates that most redundant coefficients are successfully driven to zero using sparse EKI, while there are still some non-zero redundant coefficients in the system identified by standard EKI.
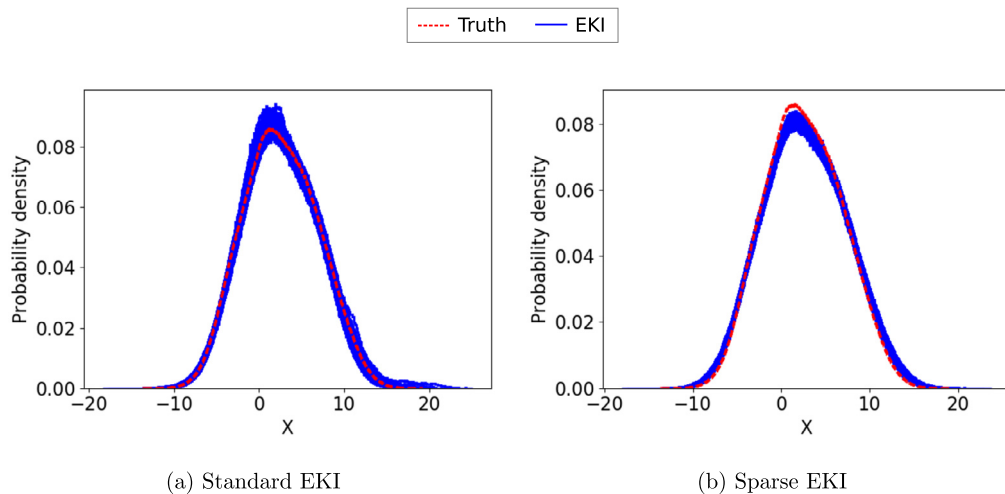
(a) Standard EKI

(b) Sparse EKI

Fig. 8. Invariant measure for single-scale Lorenz 96 system found by using (a) standard EKI and (b) sparse EKI.

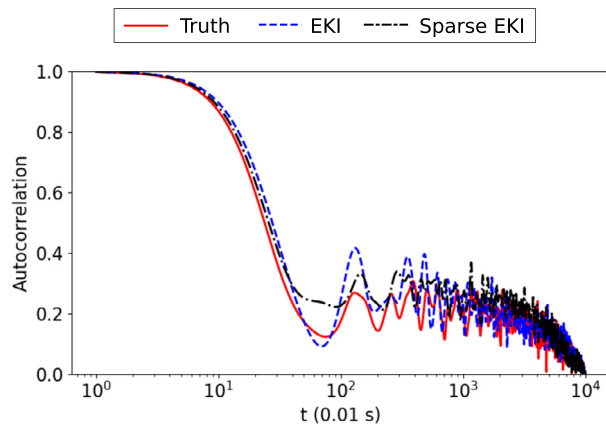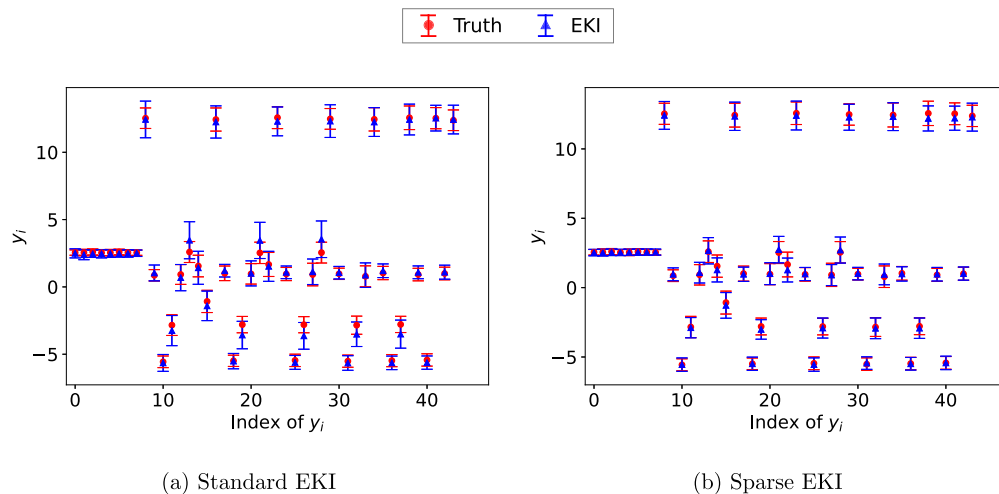**Fig. 9.** Autocorrelation for single-scale Lorenz 96 system found by using standard EKI and sparse EKI.

(a) Standard EKI

(b) Sparse EKI

Fig. 10. First two moments of state X for multi-scale Lorenz 96 system found by using (a) standard EKI and (b) sparse EKI.
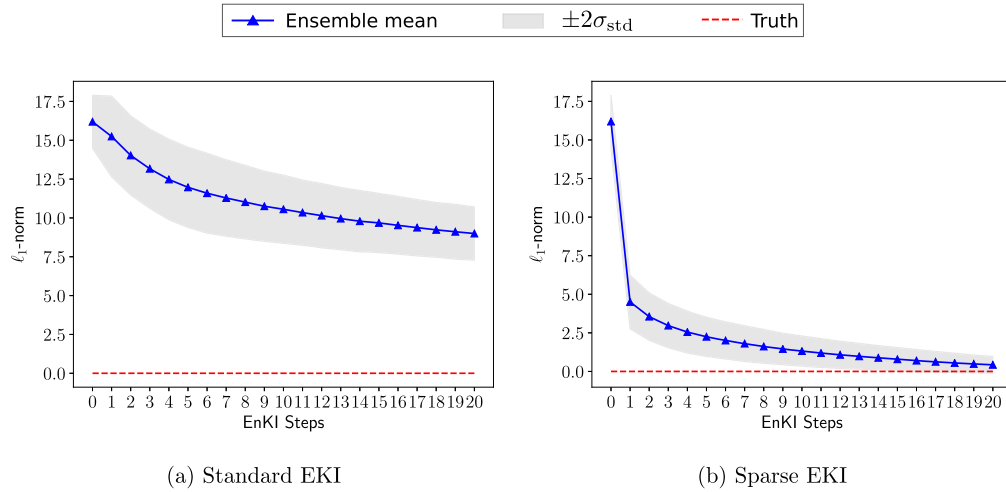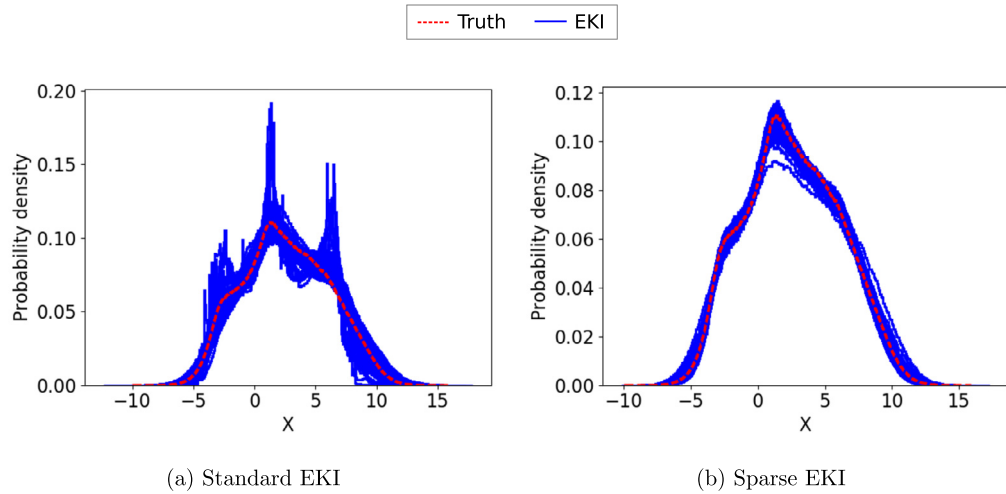
Fig. 11. ℓ_1-norm of redundant coefficients for multi-scale Lorenz 96 system found by using (a) standard EKI and (b) sparse EKI.

Fig. 12. Invariant measure for multi-scale Lorenz 96 system found by using (a) standard EKI and (b) sparse EKI.

The generalization capability of the identified systems is investigated by evaluating the invariant measure. As presented in Fig. 12, the invariant measure of the system identified by sparse EKI shows a much better agreement with the true system, indicating a better performance in the long-time limit. The comparison of the autocorrelation for a chosen ensemble is also studied in Fig. 13. It demonstrates a better agreement with the true system for the system identified by sparse EKI.

4.3. Coalescence equations

We further apply the sparse EKI to fit coalescence equations based on statistics derived from time averaging. Specifically, we study three examples: (i) a simulation study where the true system and modeled system share the same closure (Gamma distribution closure) and the same number of resolved states ($K = 2$); (ii) an example where true system and modeled system share the same closure (Gamma distribution closure), while the true system resolves more states ($K = 3$); (iii) an example where true system and modeled system share the same number of resolved states ($K = 2$), while the true system has a different closure (exponential distribution closure). For all three tests of coalescence equations, we impose the symmetry $c_{ab} = c_{ba}$ and thus fit 9 unknown coefficients (recall that we always set $r = 3$ and $c_{11} = 0$), using a data vector of dimension 5 (observing the finite-time average approximation of first and second moments). The time used for gathering averaged statistics is $T = 50$. Furthermore, we impose positivity on all learned parameters c_{ab} to ensure searching in the space of well-posed models.
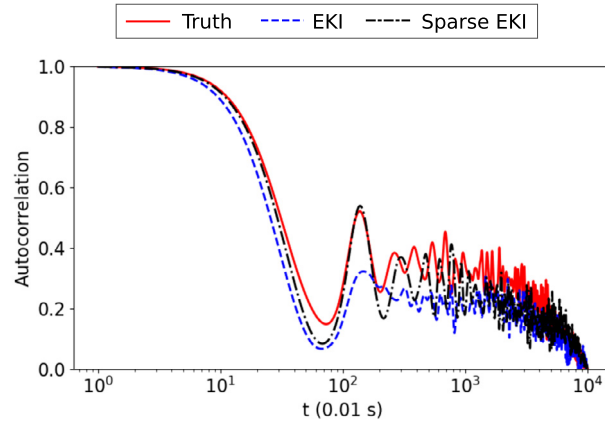
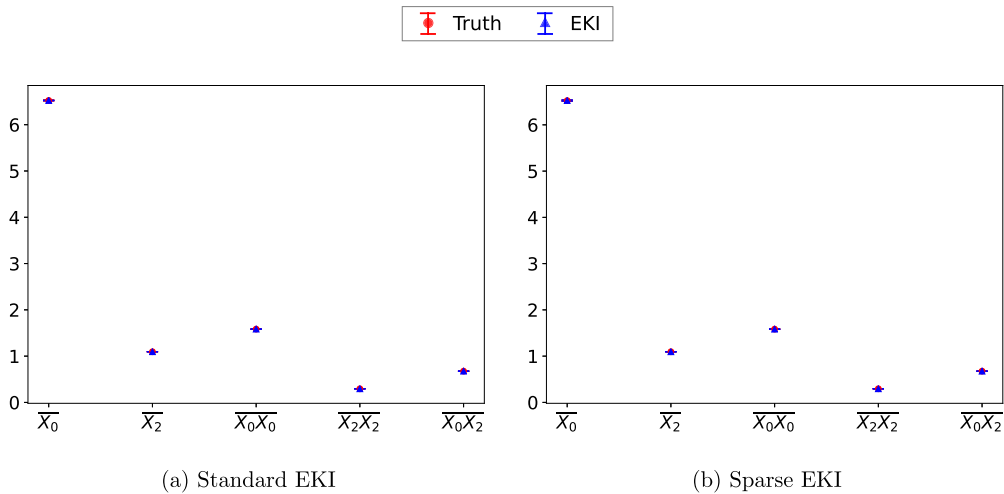**Fig. 13.** Autocorrelation for multi-scale Lorenz 96 system found by using standard EKI and sparse EKI.

(a) Standard EKI   (b) Sparse EKI

Fig. 14. First two moments of state X for coalescence equations found by using (a) standard EKI and (b) sparse EKI.

4.3.1. Simulation study

In this simulation study, the data are generated by simulating the coalescence equations in (2.15) with $K = 2$, $r = 3$ and the Gamma distribution closure in (2.16). The goal is to fit a model with the same K, r, and closure by using EKI to estimate unknown coefficients c_{ab}. The initial ensemble of unknown coefficients c_{ab} are uniformly drawn from $[-1, 1]$. The sparsity promoting parameters γ (optimization) and $\sqrt{2\lambda}$ (thresholding) are chosen as 0.6 and 0.1. We use 10 EKI iterations. Results are presented in Figs. 14 to 17.

The comparison of moments data is presented in Fig. 14, which shows that the system identified by using either standard EKI or sparse EKI can have a very good agreement with the true system in terms of matching the first two moments of simulated states. However, it is clear in Fig. 15 that the sets of parameters c_{ab} identified by standard EKI and sparse EKI are quite different. The ℓ_1-norm of redundant coefficients in Fig. 15a indicates that some of the redundant coefficients are still non-zero for the system identified by standard EKI, while all redundant coefficients are driven to zero as presented in Fig. 15b by using sparse EKI.

The comparison of the non-zero coefficient c_{00} in the true system is presented in Fig. 16. The ensemble mean of the estimated parameter matches with its true value using either standard EKI or sparse EKI, while the result of sparse EKI demonstrates better convergence of the ensemble to the true value.

We further investigate the generalization capability of EKI identified systems by comparing the simulated trajectories of states with an initial condition different from the training set. It can be seen in Fig. 17 that non-zero redundant coefficients and the disagreement of c_{00} among ensemble members do have a negative effect upon the generalization capability of the identified system, as the ensemble of simulated trajectories start to diverge after some time. On the other hand, the system identified by sparse EKI shows a much better agreement with the true trajectories in Fig. 17b, even though the initial condition in this test is different from the one used in the training of the sparse model.
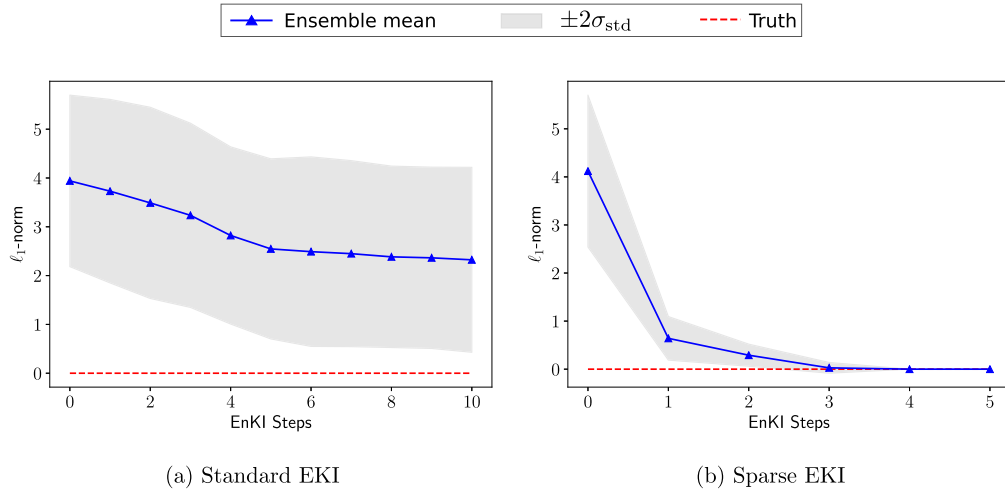
Fig. 15. ℓ_1-norm of redundant coefficients for coalescence equations found by using (a) standard EKI and (b) sparse EKI.
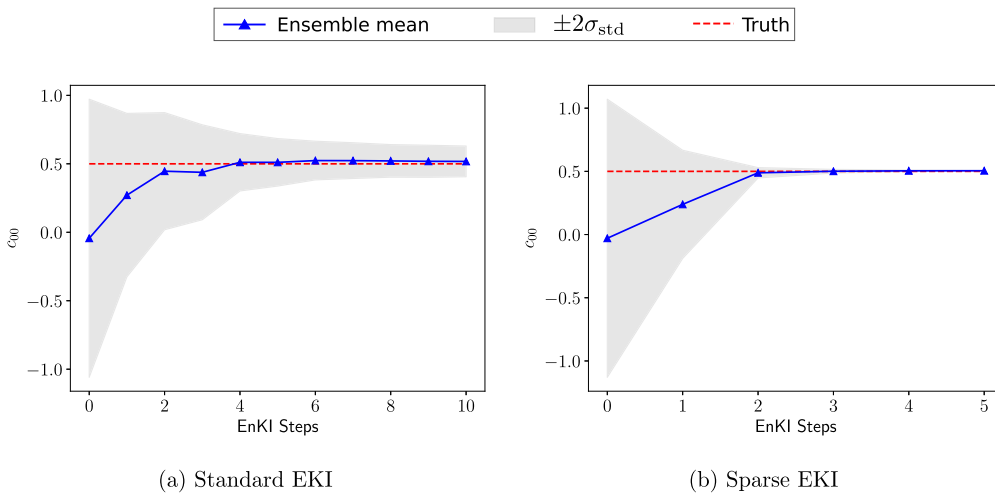

Fig. 16. Non-zero parameter for coalescence equations found by using (a) standard EKI and (b) sparse EKI.

4.3.2. Higher-order closure data

We now perform a more realistic study, in which the data are generated by simulating the coalescence equations in (2.15) with $K = 3$, $r = 3$ and the Gamma distribution closure in (2.16). The goal is to fit a model with the same r and closure but different K, namely $K = 2$, using EKI to estimate unknown coefficients c_{ab}. The initial ensemble of unknown coefficients c_{ab} is uniformly drawn from $[-1, 1]$. The sparsity promoting parameters γ (optimization) and $\sqrt{2\lambda}$ (thresholding) are chosen as 1 and 0.1. We use 10 EKI iterations. Results are presented in Figs. 18 to 21.

The comparison of data in Fig. 18 shows a comparable performance of the identified system by using either standard EKI or sparse EKI. However, the ℓ_1-norm of all coefficients is significantly different (as presented in Fig. 19). It shows that sparse EKI leads to a set of parameters with smaller ℓ_1-norm. However, we cannot directly tell whether such a set of parameters is better, since the identified system has a closure distribution different from the one of the true system.

Therefore, we investigate the performances of the EKI identified systems by studying the generalization capability in Fig. 20, i.e., simulating identified systems with an initial condition different from the training data. It is clear in Fig. 20 that the simulated trajectories of the system identified by sparse EKI agree more closely with the trajectories of the true system.

We further try to improve the performance of the identified system by using training sets with different initial conditions, noting that the coalescence equations are not ergodic, and the initial condition does have an effect on the system prediction. Specifically, we use two training sets with initial conditions $(X_0, X_1, X_2) = (10, 2, 0.6)$ and $(X_0, X_1, X_2) = (10, 2, 2)$, and we then test the performance of the identified systems with a different initial condition $(X_0, X_1, X_2) = (10, 2, 1)$. The results in Fig. 21 show that the identified systems with multiple training sets provide better agreement of simulated trajectories with the true system, and the improvement of performance is more significant for the system identified by standard EKI. This is not surprising since we still fit 9 unknown coefficients here but with twice the data (10 elements in total).
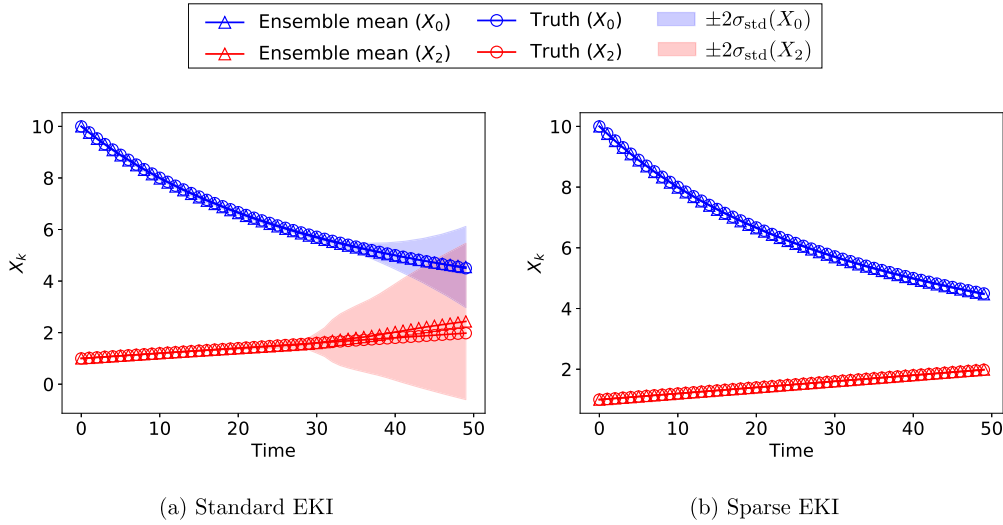
Fig. 17. Simulated states for coalescence equations with coefficients found by using (a) standard EKI and (b) sparse EKI. The initial condition of the training dataset is $(X_0, X_1, X_2) = (10, 2, 0.6)$, and the initial condition of the simulations here is $(X_0, X_1, X_2) = (10, 2, 1)$.
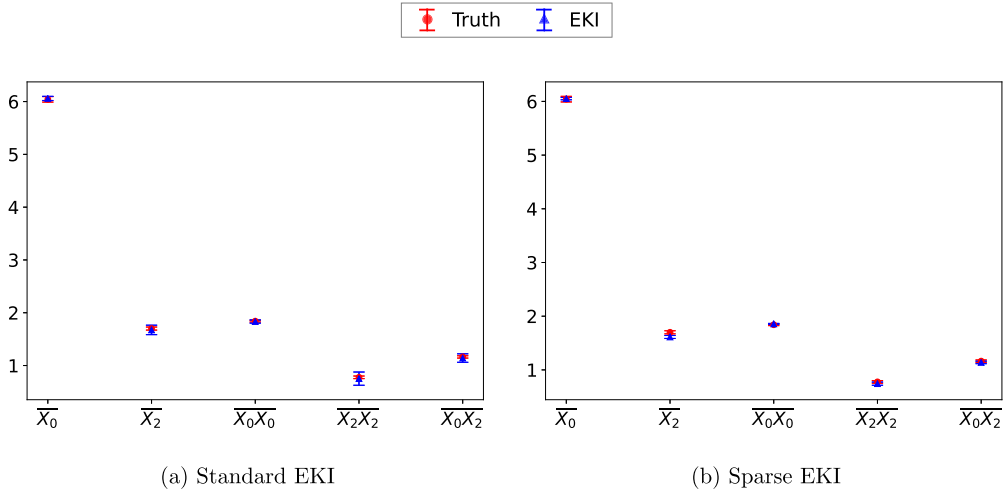

Fig. 18. First two moments of state X for coalescence equations found by using (a) standard EKI and (b) sparse EKI. The data are generated by coalescence equations with a higher-order closure ($K = 3$).

4.3.3. Gamma versus exponential closure data

We perform a further study where the true system and the modeled system have different closures. Specifically, the data are generated by simulating the coalescence equations in (2.15) with $K = 2$, $r = 3$, and with the exponential distribution closure in (2.17). The goal is to fit a model with the same K and r but with a Gamma distribution closure, using EKI to estimate unknown coefficients c_{ab}. The initial ensemble of unknown coefficients c_{ab} is uniformly drawn from $[-1, 1]$. The sparsity promoting parameters γ (optimization) and $\sqrt{2\lambda}$ (thresholding) are chosen as 1 and 0.1. We use 10 EKI iterations. Results are presented in Figs. 22 to 25.

The comparison of data in Fig. 22 shows larger uncertainties for the results of standard EKI, while the ensemble mean agrees relatively well with the data of the true system. The larger uncertainties can also be seen in Fig. 23: the ℓ_1-norm of all coefficients estimated using standard EKI remains relatively large, while the sparse EKI identifies another set of parameters with smaller ℓ_1-norm.

We then investigate the performance of EKI identified systems by simulating state trajectories with an initial condition different from the training data. The comparison of simulated trajectories is presented in Fig. 24. Although the ensemble mean of either standard EKI or sparse EKI has similar agreement with the trajectories of the true system, there are larger uncertainties in the ensemble of simulated trajectories for the results of standard EKI.

We further demonstrate that the performance of EKI identified systems can be improved by using multiple training sets. Specifically, two training sets are used with initial conditions $(X_0, X_1, X_2) = (10, 2, 0.6)$ and $(X_0, X_1, X_2) = (20, 2, 0.6)$,
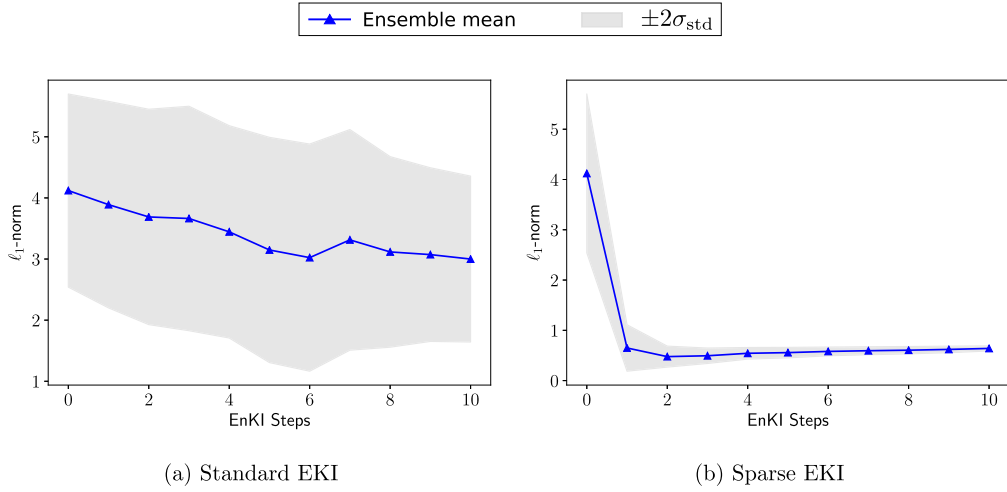
(a) Standard EKI

(b) Sparse EKI

Fig. 19. ℓ_1-norm of all coefficients for coalescence equations found by using (a) standard EKI and (b) sparse EKI. The data are generated by coalescence equations with a higher order closure ($K = 3$).
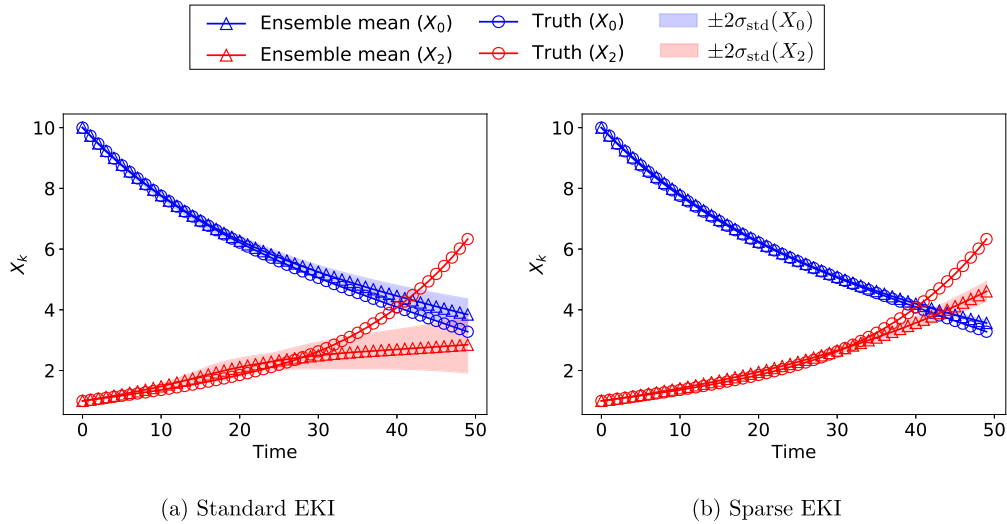

(a) Standard EKI

(b) Sparse EKI

Fig. 20. Simulated states for coalescence equations with coefficients found by using (a) standard EKI and (b) sparse EKI. The data are generated by coalescence equations with a higher-order closure ($K = 3$). The initial condition of the training dataset is $(X_0, X_1, X_2) = (10, 2, 0.6)$, and the initial condition of the simulations here is $(X_0, X_1, X_2) = (10, 2, 1)$.

and the initial condition of the test presented in Fig. 25 is $(X_0, X_1, X_2) = (15, 2, 0.6)$. Compared to the trajectories of EKI identified systems with a single training set in Fig. 24, the agreement of simulated trajectories with the true ones is generally better in Fig. 25 where multiple training set being used.

4.4. Kuramoto-Sivashinsky equation

We conclude the numerical study by applying the sparse EKI to fit the Kuramoto-Sivashinsky Equation (2.20). We first observe that applying the standard EKI approach to learn the equation, from within the class represented in (2.21) and using the same data as for sparse EKI, leads to a solution as presented in Table 2. It fails to find a solution from within the class (2.21) that is close to the data-generating equation (2.20), clearly motivating the need for the sparse EKI method, results from which are also shown in the same table.

We now turn to the sparse setting in more detail. Working within the class of models (2.21) requires 10 unknown coefficients $\{\alpha_j, \beta_j\}_{j=1}^5$ to be learnt. To do this, we use a data vector y of dimension 114. Specifically, the data vector consists of: (i) the first to fourth moments at eight locations $\{x_j\}_{j=1}^8$ that are evenly distributed across the range of x, namely $\{\overline{u_j}, \{\overline{u_j u_k}\}_{k=1}^8, \overline{u_j u_j u_j}, \overline{u_j u_j u_j u_j}\}_{j=1}^8$, giving a total moment-data vector of size $8 + 36 + 8 + 8 = 60$; (ii) temporal autocorrelation of $u(x_j, t)$ at the same eight locations of x and using five points in time, giving a total autocorrelation-data

(a) Standard EKI   (b) Sparse EKI
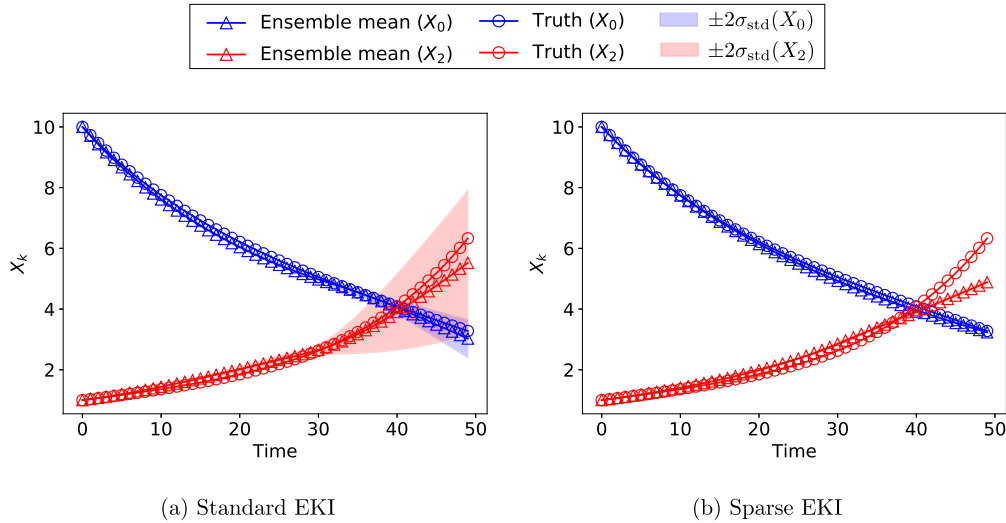
Fig. 21. Simulated states for coalescence equations with coefficients found by using (a) standard EKI and (b) sparse EKI. Two datasets are generated by coalescence equations with a higher order closure ($K = 3$). The initial conditions of the training datasets are $(X_0, X_1, X_2) = (10, 2, 0.6)$ and $(X_0, X_1, X_2) = (10, 2, 2)$, and the initial condition of the simulations here is $(X_0, X_1, X_2) = (10, 2, 1)$.
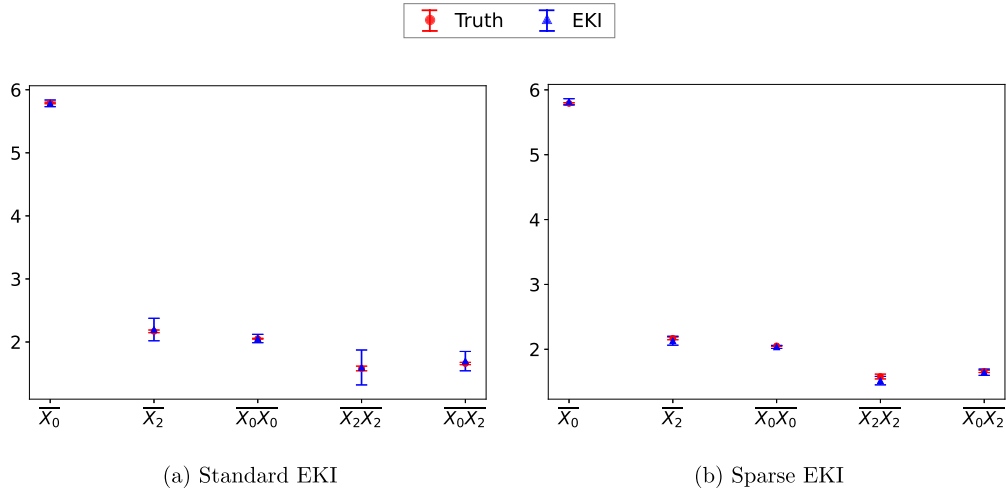

(a) Standard EKI   (b) Sparse EKI

Fig. 22. First two moments of state X for coalescence equations found by using (a) standard EKI and (b) sparse EKI. The data are generated by coalescence equations with an exponential closure.

Table 2
Mean value of coefficients estimated by standard EKI and sparse EKI.

Linear terms	$\partial_x^1 u$	$\partial_x^2 u$	$\partial_x^3 u$	$\partial_x^4 u$	$\partial_x^5 u$
Coefficient (Standard EKI)	-0.330	1.385	0.659	1.262	-0.130
Coefficient (Sparse EKI)	0	1.020	0	1.020	0
Coefficient (Truth)	0	1	0	1	0
Non-linear terms	$u\partial_x u$	$u^2\partial_x u$	$u^3\partial_x u$	$u^4\partial_x u$	$u^5\partial_x u$
Coefficient (Standard EKI)	1.420	0.224	-0.455	0.104	0.149
Coefficient (Sparse EKI)	1.024	0	0	0	0
Coefficient (Truth)	1	0	0	0	0

vector of size 40; and (iii) the time-averaged spatial correlation function at 14 locations in space x. The time used for averaging is $T = 1000$, and all simulations are performed on the torus $[0, L]$ with $L = 128$. In this case, we use an ensemble size of 200. The initial ensemble of unknown coefficients α_j and β_j are uniformly drawn from $[0, 5]$. The sparsity promoting parameters γ (optimization) and $\sqrt{2\lambda}$ (thresholding) are chosen as 4 and 0.1. We use 30 EKI iterations. The initial condition is set as $\cos(x) + 0.1 \times \cos(x/16) \times (1 + 2 \times \sin(x/16))$, plus a small noise uniformly drawn from $[0, 10^{-3}]$. Details of the
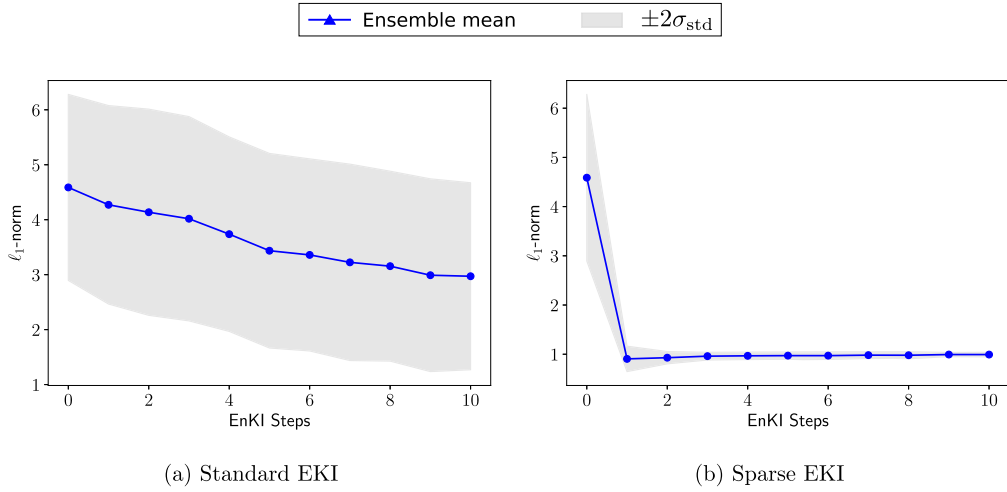
Fig. 23. ℓ_1-norm of all coefficients for coalescence equations found by using (a) standard EKI and (b) sparse EKI. The data are generated by coalescence equations with an exponential closure.
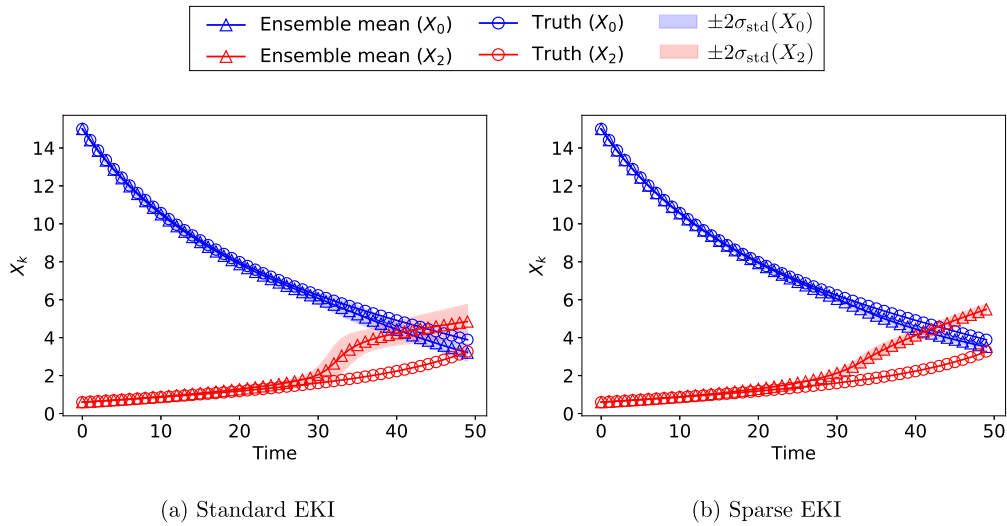

Fig. 24. Simulated states for coalescence equations with coefficients found by using (a) standard EKI and (b) sparse EKI. The data are generated by coalescence equations with an exponential closure. The initial condition of the training dataset is $(X_0, X_1, X_2) = (10, 2, 0.6)$, and the initial condition of the simulations here is $(X_0, X_1, X_2) = (15, 2, 0.6)$.

methods employed to solve the extended K-S equation (2.21) are described in Appendix A, including the Fourier-based approach to finding the spatial correlation function.

We run sparse EKI algorithm in two phases (see Section 3.2). Results of the first phase (with all ten basis functions) are presented in Figs. 26 and 27, and results of the second phase (using a reduced number of four basis functions, informed by the first phase of the algorithm, are presented in Figs. 28 and 29.

The comparison of data is presented in Fig. 26 for the first sparse EKI phase. The comparison of the autocorrelation results at the eight locations is similar, and thus we only present the autocorrelation results at $x = 0$. In terms of all three types of data, there are some mismatches between the results of sparse EKI and the true data. In order to evaluate the performance of sparse EKI more precisely, we present the learning of three necessary coefficients (α_2, α_4, and β_1) and the ℓ_1-norm of redundant coefficients in Fig. 27. It is clear that there are some biases in the estimated parameters α_2 and α_4, while the sparse EKI successfully drives the ℓ_1-norm of redundant coefficients close to zero.

In order to improve the accuracy of the estimated parameters in Fig. 27, we perform the second phase of sparse EKI only using the basis functions with non-zero coefficients (α_2, α_4, β_1, and β_3) in the first phase. The comparison of data is presented in Fig. 28 for the second phase, which shows a much better agreement with all three types of data. The estimated parameters from the second phase are presented in Fig. 29, confirming that the Kuramoto-Sivashinsky equation can be accurately identified by using sparse EKI. The results are summarized in Table 2, which demonstrates that the sparse
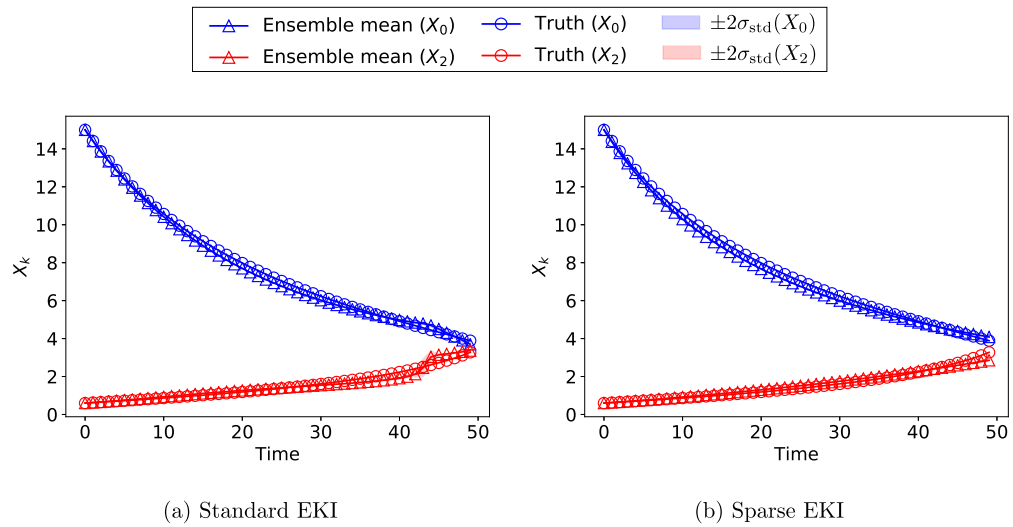
(a) Standard EKI   (b) Sparse EKI

Fig. 25. Simulated states for coalescence equations with coefficients found by using (a) standard EKI and (b) sparse EKI. Two datasets are generated by coalescence equations with an exponential closure. The initial conditions of the training datasets are $(X_0, X_1, X_2) = (10, 2, 0.6)$ and $(X_0, X_1, X_2) = (20, 2, 0.6)$, and the initial condition of the simulations here is $(X_0, X_1, X_2) = (15, 2, 0.6)$.
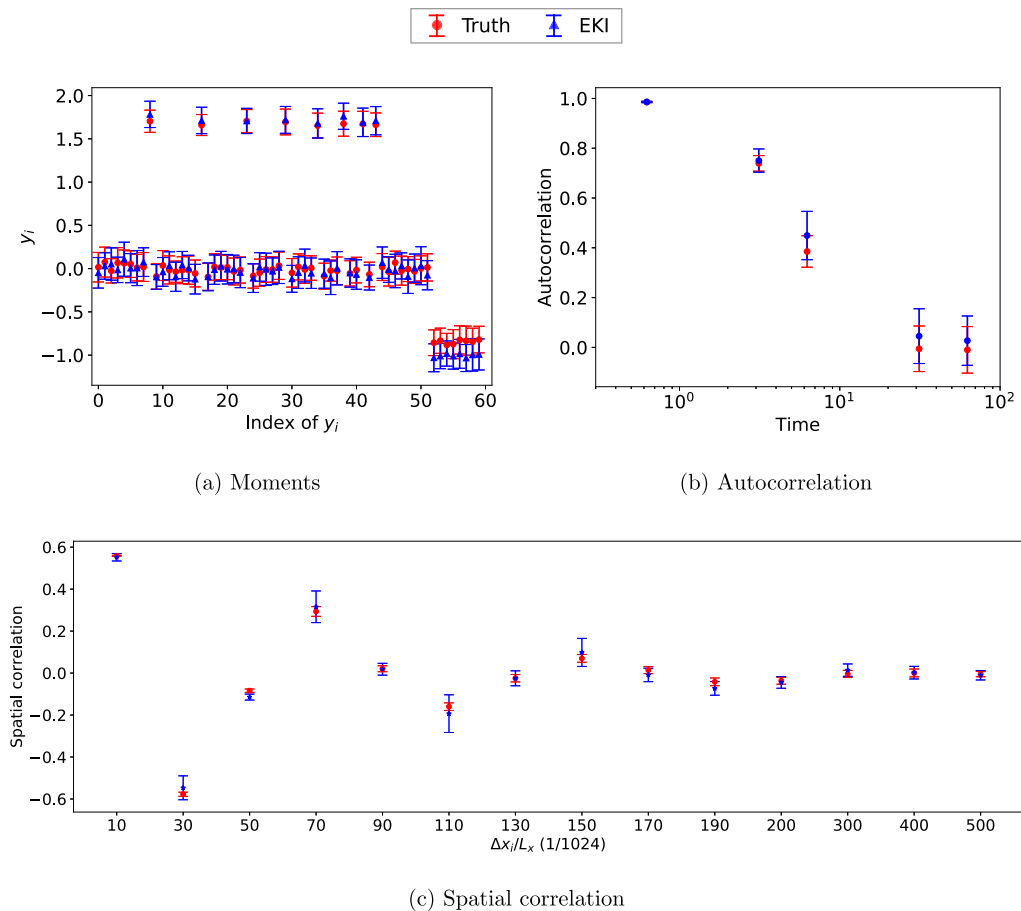

(a) Moments   (b) Autocorrelation

(c) Spatial correlation

Fig. 26. Comparison between the data from the true system and results of the first sparse EKI, including (a) first four moments, (b) autocorrelation at $x = 0$, and (c) time-averaged spatial correlation.
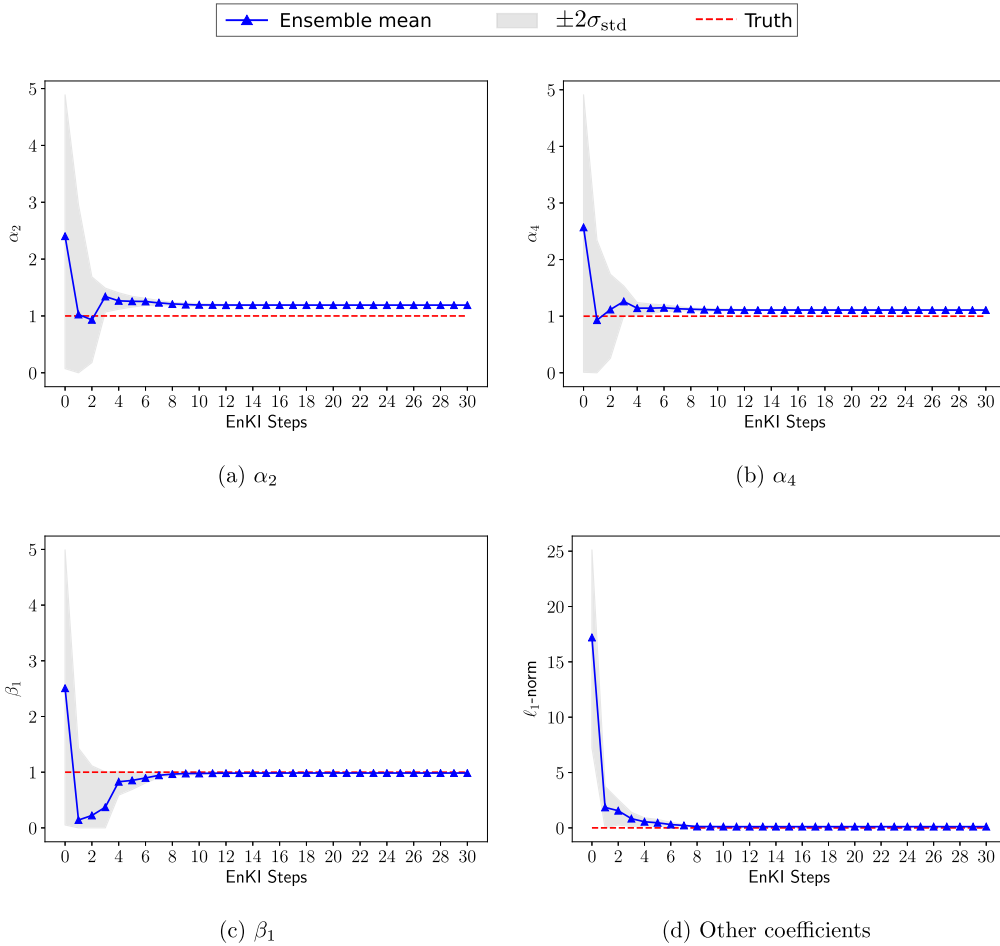
Fig. 27. Estimated coefficients from the first EKI, including (a)–(c) necessary coefficients of Kuramoto-Sivashinsky Equation (α_2, α_4, and β_1), and (d) the ℓ_1-norm of other coefficients. There are four nonzero coefficients (α_2, α_4, β_1, and β_3) in the results of first EKI.

EKI method correctly recovers the three non-zero coefficients, to an accuracy of less than 2.5%, and correctly zeros out all other coefficients; in contrast, the standard EKI finds a non-sparse fit to the data in which all 10 basis coefficients are active. This concluding example demonstrates both the power of sparsity promoting learning of dynamical systems, and the ability of the sparse EKI method to learn dynamical systems from indirect, partial and nonlinear observations.

5. Conclusions

We have demonstrated that sparsity may be naturally incorporated into ensemble Kalman-based inversion methods, leading to the sparse EKI algorithm. The focus of the paper was on learning dynamical models from indirect, partial, and nonlinear observations, because the solution of such inverse problems in the sparse setting has been an outstanding challenge. We focus on time-averaged data as a canonical example of such data. The numerical results presented showcase the success of discovering dynamical models in a variety of different examples, demonstrating that sparse learning for model discovery from time-averaged functions of states can be effectively achieved. The proposed sparse learning methodology extends the scope of data-driven discovery of dynamical models from linear observation operators to previously challenging applications where the observation operator is nonlinear. The methodology may in principle be used for the solution of a wide class of nonlinear inverse problems in which sparse solutions are sought. As with existing methods to find sparse solutions of *linear* inverse problems, the core computational task is a quadratic programming problem, subject to linear inequality constraints, and therefore easily implemented. Remarkably, this same computational task allows for solution of *nonlinear* inverse problems when using the proposed sparse EKI method.

Directions for future research stemming from our work include:

- application of the method to other nonlinear inverse problems where sparse learning from a dictionary of functions is valuable;
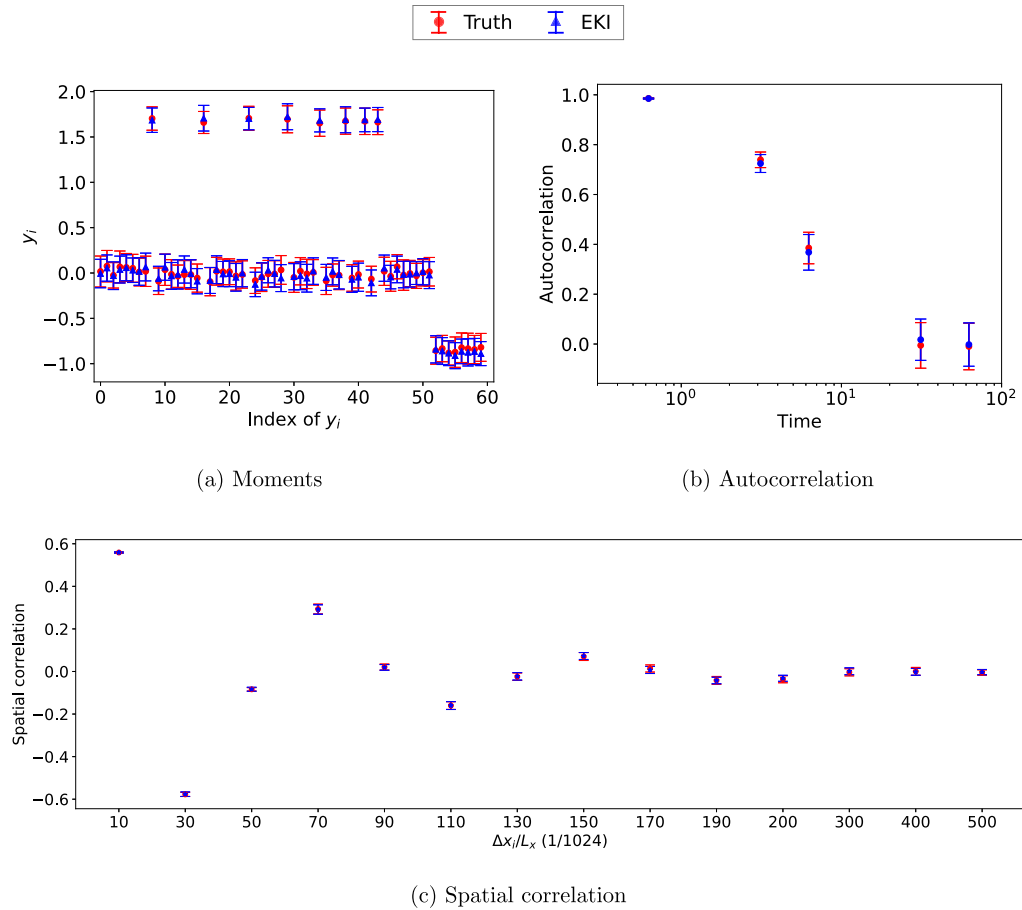
(a) Moments

(b) Autocorrelation

(c) Spatial correlation

Fig. 28. Comparison between the data from the true system and results of the second sparse EKI, including (a) first four moments, (b) autocorrelation at $x = 0$, and (c) time-averaged spatial correlation.

- development of theory to support the use of the algorithm, noting however that, even in the absence of constraints and imposition of sparsity, the theoretical underpinnings of ensemble inversion methods are only starting to be understood [39,65];
- detailed study of the use of different algorithms for the imposition of sparsity on the basic quadratic programming task, which is undertaken iteratively during ensemble Kalman inversion;
- careful comparison of ensemble Kalman inversion with other sparsity imposing methods for solving the nonlinear inverse problem of learning dynamical systems from data in time-averaged form.

The Julia implementation of standard EKI and Sparse EKI can be found in:
https://github.com/CliMA/EnsembleKalmanProcesses.jl.

CRediT authorship contribution statement

Tapio Schneider: Conceptualization, Supervision, Writing – review & editing. **Andrew M. Stuart:** Conceptualization, Methodology, Supervision, Writing – review & editing. **Jin-Long Wu:** Conceptualization, Investigation, Methodology, Software, Validation, Visualization, Writing – original draft.

Declaration of competing interest

The authors declare that they have no known competing financial interests or personal relationships that could have appeared to influence the work reported in this paper.

Data availability

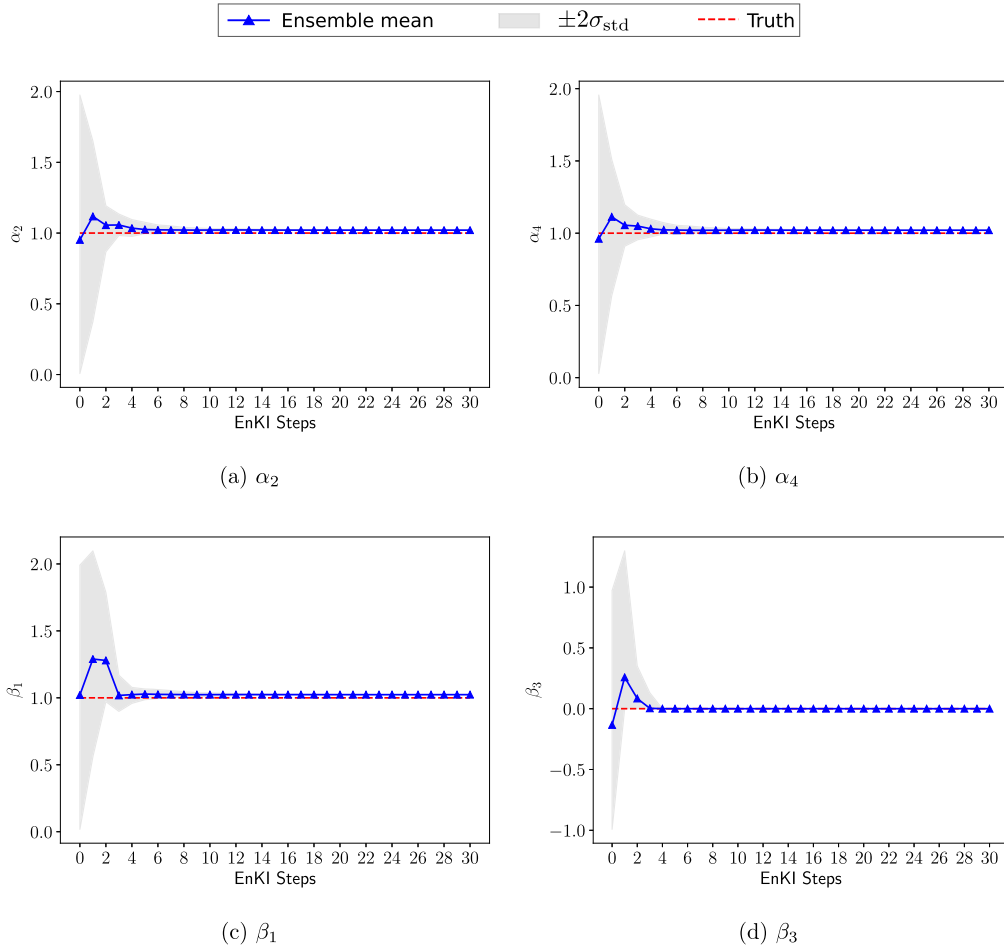The authors have shared the link to data/code at the Attach File step.

(a) α_2

(b) α_4

(c) β_1

(d) β_3

Fig. 29. Estimated coefficients from the second sparse EKI, including (a)–(c) necessary coefficients of Kuramoto-Sivashinsky Equation (α_2, α_4, and β_1), and (d) the redundant coefficient β_3.

Acknowledgements

Appendix A. Numerical solution of the extended K-S equation

We consider the Extended Kuramoto–Sivashinsky (E-K-S) equation on a periodic domain in one dimension:

$$\partial_t u = -\sum_{j=1}^{5}\Big(\alpha_j \partial_x^j u + \beta_j u^j \partial_x u\Big), \quad x \in \mathbb{T}^L,$$

$$u|_{t=0} = u_0;$$

(A.1)

here $\mathbb{T}^L$ denotes the torus $[0, L]$.

The E-K-S equation is semilinear (provided at least one coefficient of spatial derivative two or more is non-zero) and it is useful to write it in the form

$$\partial_t u = \mathcal{L}u + \mathcal{N}(u),$$

(A.2)

where

$$\mathcal{L}u = -\sum_{j=1}^{5} \alpha_j \partial_x^j u,$$

$$\mathcal{N}(u) = -\sum_{j=1}^{5} \frac{\beta_j}{(j+1)} \partial_x(u^{j+1}).$$

(A.3)

Using the Crank-Nicolson/Adams-Bashforth scheme, the above equation can be discretized as

$$\frac{u_{(n+1)} - u_{(n)}}{\Delta t} = \mathcal{L}\frac{u_{(n+1)} + u_{(n)}}{2} + \frac{3}{2}\mathcal{N}(u_{(n)}) - \frac{1}{2}\mathcal{N}(u_{(n-1)}),$$

(A.4)

where $u_{(n)} = u(x, n\Delta t)$. We introduce the Fourier transform in the spatial domain:

$$\hat{u}(\xi) = \mathcal{F}(u) = \int_0^L u(x)e^{-2\pi i x\xi} dx.$$

(A.5)

Using this notation we obtain the discretization:

$$\frac{\hat{u}_{(n+1)} - \hat{u}_{(n)}}{\Delta t} = \hat{\mathcal{L}}\Big(\frac{\hat{u}_{(n+1)} + \hat{u}_{(n)}}{2}\Big) + \frac{3}{2}\hat{\mathcal{N}}(\hat{u}_{(n)}) - \frac{1}{2}\hat{\mathcal{N}}(\hat{u}_{(n-1)}),$$

(A.6)

where

$$\hat{\mathcal{L}}\hat{u} = -\sum_{j=1}^{5} \alpha_j (2\pi i\xi)^j \hat{u},$$

$$\hat{\mathcal{N}}(\hat{u}) = -\sum_{j=1}^{5} \frac{2\pi i\xi\beta_j}{(j+1)} \mathcal{F}\Big(\big(\mathcal{F}^{-1}(\hat{u})\big)^{j+1}\Big),$$

(A.7)

and where $\mathcal{F}^{-1}$ denotes the inverse Fourier transform. In this work, the spatial domain is discretized by 1024 points that are evenly distributed, and fast Fourier transform is used to map between spatial domain and spectral domain. There is no further truncation in the spectral domain, and thus we have 1024 terms in the spectral domain. Note that if $\alpha_4 > 0$ then $\lim_{|\xi|\to\infty} Re(\hat{\mathcal{L}}) = -\infty$ which makes the equation well-posed. The discretization in (A.6) can be further formulated as

$$\Big(I - \frac{\Delta t}{2}\hat{\mathcal{L}}\Big)\hat{u}_{(n+1)} = \Big(I + \frac{\Delta t}{2}\hat{\mathcal{L}}\Big)\hat{u}_{(n)} + \frac{3\Delta t}{2}\hat{\mathcal{N}}(\hat{u}_{(n)}) - \frac{\Delta t}{2}\hat{\mathcal{N}}(\hat{u}_{(n-1)}).$$

(A.8)

Alternatively, a standard integrating factor method can be obtained by introducing the Fourier transform in the spatial domain and rewriting the Fourier transform of (A.2) as

$$\partial_t\Big(e^{-\hat{\mathcal{L}}t}\hat{u}\Big) = e^{-\hat{\mathcal{L}}t}\hat{N}(\hat{u}).$$

(A.9)

This equation can be solved numerically by using the second-order Adams–Bashforth scheme to obtain

$$\hat{u}_{(n+1)} = e^{\hat{\mathcal{L}}\Delta t}\hat{u}_{(n)} + \frac{3\Delta t}{2}e^{\hat{\mathcal{L}}\Delta t}\hat{\mathcal{N}}(\hat{u}_{(n)}) - \frac{\Delta t}{2}e^{2\hat{\mathcal{L}}\Delta t}\hat{\mathcal{N}}(\hat{u}_{(n-1)}).$$

(A.10)

The two algorithms (A.8), (A.10) may be found in [77].

In this work, numerical clipping is implemented at every time step to avoid possible blow-up induced by the numerical discretization (A.8) or (A.10):

$$[\hat{u}_{(n+1)}] = \mathcal{F}\Big(\max\Big(\min\Big(\mathcal{F}^{-1}(\hat{u}_{(n+1)}), u_{(n+1)}^{max}\Big), u_{(n+1)}^{min}\Big)\Big),$$

(A.11)

where $u_{(n+1)}^{max}$ and $u_{(n+1)}^{min}$ are upper and lower bounds imposed on the simulated state in the spatial domain. We use constant upper and lower bounds across the whole spatial domain, and the numerical clipping is imposed pointwise at every grid point in the spatial domain. In practice, the numerical clipping can also prevent the failure of sparse EKI when the system with intermediate estimated coefficients is unstable. However, it should be noted that the clipping may lead to estimated coefficients that collapse at incorrect values; such undesirable behavior is addressed by performing sparse EKI again upon the reduced system from the previous sparse EKI. Both algorithms (A.8), (A.10), with clipping, were used, initially, to test the robustness of results to choice of time-stepper; having verified this robustness, all results presented in the paper use algorithm (A.8).
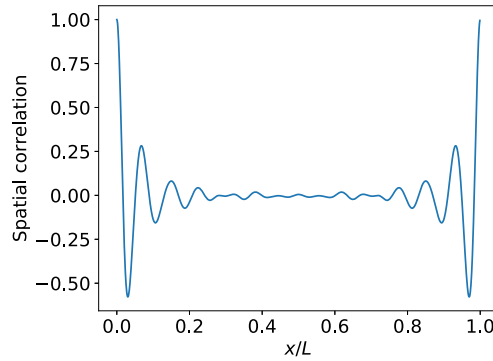
Fig. A.30. The time-averaged spatial correlation of the simulated states of K-S equation. Normalization has been performed to set the largest value to 1.

Using algorithm (A.8) we compute the time-averaged spatial correlation function defined by

$$C(x) = \frac{1}{T} \int_0^T \int_0^L u(z,t) u(z+x,t) dz dt. \tag{A.12}$$

Notice that

$$(\mathcal{F}C)(\xi) = \frac{1}{T} \int_0^T |(\mathcal{F}u)(\xi,t)|^2 dt$$

facilitating straightforward computation in Fourier space. The function $C(x)$ is shown in Fig. A.30. It is used as part of the definition of G, along with moments and autocorrelation information, from which we learn parameters.

References

[1] D.L. Donoho, Compressed sensing, IEEE Trans. Inf. Theory 52 (4) (2006) 1289–1306.
[2] E.J. Candes, J.K. Romberg, T. Tao, Stable signal recovery from incomplete and inaccurate measurements, Commun. Pure Appl. Math. 59 (8) (2006) 1207–1223.
[3] E.J. Candes, M.B. Wakin, S.P. Boyd, Enhancing sparsity by reweighted ℓ_1 minimization, J. Fourier Anal. Appl. 14 (5–6) (2008) 877–905.
[4] A.M. Bruckstein, D.L. Donoho, M. Elad, From sparse solutions of systems of equations to sparse modeling of signals and images, SIAM Rev. 51 (1) (2009) 34–81.
[5] F. Santosa, W.W. Symes, Linear inversion of band-limited reflection seismograms, SIAM J. Sci. Stat. Comput. 7 (4) (1986) 1307–1330.
[6] R. Tibshirani, Regression shrinkage and selection via the lasso, J. R. Stat. Soc. B 58 (1) (1996) 267–288.
[7] R. Tibshirani, Regression shrinkage and selection via the lasso: a retrospective, J. R. Stat. Soc., Ser. B, Stat. Methodol. 73 (3) (2011) 273–282.
[8] I. Goodfellow, Y. Bengio, A. Courville, Deep Learning, MIT Press, 2016.
[9] S.L. Brunton, J.L. Proctor, J.N. Kutz, Discovering governing equations from data by sparse identification of nonlinear dynamical systems, Proc. Natl. Acad. Sci. USA 113 (15) (2016) 3932–3937.
[10] S.H. Rudy, S.L. Brunton, J.L. Proctor, J.N. Kutz, Data-driven discovery of partial differential equations, Sci. Adv. 3 (4) (2017) e1602614.
[11] H. Schaeffer, R. Caflisch, C.D. Hauck, S. Osher, Sparse dynamics for partial differential equations, Proc. Natl. Acad. Sci. USA 110 (17) (2013) 6634–6639.
[12] H. Schaeffer, Learning partial differential equations via data discovery and sparse optimization, Proc. R. Soc. A, Math. Phys. Eng. Sci. 473 (2197) (2017) 20160446.
[13] G. Tran, R. Ward, Exact recovery of chaotic systems from highly corrupted data, Multiscale Model. Simul. 15 (3) (2017) 1108–1129.
[14] H. Schaeffer, G. Tran, R. Ward, Extracting sparse high-dimensional dynamics from limited data, SIAM J. Appl. Math. 78 (6) (2018) 3279–3295.
[15] J. Pereira, M. Ibrahimi, A. Montanari, Learning networks of stochastic differential equations, in: Advances in Neural Information Processing Systems, 2010, pp. 172–180.
[16] L. Boninsegna, F. Nüske, C. Clementi, Sparse learning of stochastic dynamical equations, J. Chem. Phys. 148 (24) (2018) 241723.
[17] L.I. Rudin, S. Osher, E. Fatemi, Nonlinear total variation based noise removal algorithms, Physica D 60 (1–4) (1992) 259–268.
[18] R. Chartrand, Numerical differentiation of noisy, nonsmooth data, ISRN Appl. Math. (2011).
[19] P. Shaman, R.A. Stine, The bias of autoregressive coefficient estimators, J. Am. Stat. Assoc. 83 (403) (1988) 842–848.
[20] R. Martin, C. Openshaw, Autoregressive modelling in vector spaces: an application to narrow-bandwidth spectral estimation, Signal Process. 50 (3) (1996) 189–194.
[21] A. Neumaier, T. Schneider, Estimation of parameters and eigenmodes of multivariate autoregressive models, ACM Trans. Math. Softw. 27 (2001) 27–57.
[22] T. Schneider, A. Neumaier, Algorithm 808: ARfit – a Matlab package for the estimation of parameters and eigenmodes of multivariate autoregressive models, ACM Trans. Math. Softw. 27 (2001) 58–65.
[23] H. Lütkepohl, Introduction to Multiple Time Series Analysis, Springer Science & Business Media, 2013.
[24] P.J. Brockwell, R.A. Davis, S.E. Fienberg, Time Series: Theory and Methods, Springer Science & Business Media, 1991.
[25] S. Krumscheid, G.A. Pavliotis, S. Kalliadasis, Semiparametric drift and diffusion estimation for multiscale diffusions, Multiscale Model. Simul. 11 (2) (2013) 442–473.
[26] S. Krumscheid, M. Pradas, G. Pavliotis, S. Kalliadasis, Data-driven coarse graining in action: modeling and prediction of complex systems, Phys. Rev. E 92 (4) (2015) 042139.

[27] S. Kalliadasis, S. Krumscheid, G.A. Pavliotis, A new framework for extracting coarse-grained models from time series with multiscale structure, J. Comput. Phys. 296 (2015) 314–328.

[28] S. Klus, F. Nüske, S. Peitz, J.-H. Niemann, C. Clementi, C. Schütte, Data-driven approximation of the Koopman generator: model reduction, system identification, and control, Physica D 406 (2020) 132416.

[29] T. Schneider, A.M. Stuart, J.-L. Wu, Learning stochastic closures using ensemble Kalman inversion, Trans. Math. Appl. 5 (1) (2021) tnab003.

[30] B.G. Brown, R.W. Katz, A.H. Murphy, Time series models to simulate and forecast wind speed and wind power, J. Clim. Appl. Meteorol. 23 (8) (1984) 1184–1195.

[31] F. Kwasniok, G. Lohmann, Deriving dynamical models from paleoclimatic records: application to glacial millennial-scale climate variability, Phys. Rev. E 80 (6) (2009) 066104.

[32] G. Evensen, Data Assimilation: the Ensemble Kalman Filter, Springer Science & Business Media, 2009.

[33] Y. Chen, D. Oliver, Ensemble randomized maximum likelihood method as an iterative ensemble smoother, Math. Geosci. 44 (1) (2002) 1–26.

[34] A. Emerick, A. Reynolds, Investigation of the sampling performance of ensemble-based methods with a simple reservoir model, Comput. Geosci. 17 (2) (2013) 325–350.

[35] G. Evensen, Sequential data assimilation with a nonlinear quasi-geostrophic model using Monte Carlo methods to forecast error statistics, J. Geophys. Res., Oceans 99 (C5) (1994) 10143–10162.

[36] P.J. Van Leeuwen, G. Evensen, Data assimilation and inverse methods in terms of a probabilistic formulation, Mon. Weather Rev. 124 (12) (1996) 2898–2913.

[37] S. Reich, A dynamical systems framework for intermittent data assimilation, BIT Numer. Math. 51 (1) (2011) 235–249.

[38] M.A. Iglesias, K.J. Law, A.M. Stuart, Ensemble Kalman methods for inverse problems, Inverse Probl. 29 (4) (2013) 045001.

[39] C. Schillings, A.M. Stuart, Analysis of the ensemble Kalman filter for inverse problems, SIAM J. Numer. Anal. 55 (3) (2017) 1264–1290.

[40] M. Pulido, P. Tandeo, M. Bocquet, A. Carrassi, M. Lucini, Stochastic parameterization identification using ensemble Kalman filtering combined with maximum likelihood methods, Tellus A 70 (2018) 1442099, https://doi.org/10.1080/16000870.2018.1442099.

[41] M. Bocquet, J. Brajard, A. Carrassi, L. Bertino, Bayesian inference of chaotic dynamics by merging data assimilation, machine learning and expectation-maximization, Found. Data Sci. 2 (2020) 55–80, https://doi.org/10.3934/fods.2020004.

[42] D.J. Albers, P.-A. Blancquart, M.E. Levine, E.E. Seylabi, A. Stuart, Ensemble Kalman methods with constraints, Inverse Probl. 35 (9) (2019) 095007.

[43] M.A. Iglesias, A regularizing iterative ensemble Kalman method for PDE-constrained inverse problems, Inverse Probl. 32 (2) (2016) 025002.

[44] N.K. Chada, A.M. Stuart, X.T. Tong, Tikhonov regularization within ensemble Kalman inversion, SIAM J. Numer. Anal. 58 (2) (2020) 1263–1294.

[45] N.K. Chada, C. Schillings, S. Weissmann, On the incorporation of box-constraints for ensemble Kalman inversion, arXiv preprint, arXiv:1908.00696.

[46] J. Wu, J.-X. Wang, S.C. Shadden, Adding constraints to Bayesian inverse problems, in: Proceedings of the AAAI Conference on Artificial Intelligence, vol. 33, 2019, pp. 1666–1673.

[47] X. Zhang, C. Michelén-Ströfer, H. Xiao, Regularized ensemble Kalman methods for inverse problems, J. Comput. Phys. (2020) 109517.

[48] C.A.M. Ströfer, X.-L. Zhang, H. Xiao, O. Coutier-Delgosha, Enforcing boundary conditions on physical fields in Bayesian inversion, Comput. Methods Appl. Mech. Eng. 367 (2020) 113097.

[49] Y. Lee, ℓ_p regularization for ensemble Kalman inversion, SIAM J. Sci. Comput. 43 (5) (2021) A3417–A3437.

[50] T. Schneider, S. Lan, A.M. Stuart, J. Teixeira, Earth system modeling 2.0: a blueprint for models that learn from observations and targeted high-resolution simulations, Geophys. Res. Lett. 44 (24) (2017) 12–396.

[51] E.N. Lorenz, Deterministic nonperiodic flow, J. Atmos. Sci. 20 (2) (1963) 130–141.

[52] X. Mao, Stochastic Differential Equations and Applications, Elsevier, 2007.

[53] J.C. Mattingly, A.M. Stuart, D.J. Higham, Ergodicity for SDEs and approximations: locally Lipschitz vector fields and degenerate noise, Stoch. Process. Appl. 101 (2) (2002) 185–232.

[54] E.N. Lorenz, Predictability: a problem partly solved, in: Proc. Seminar on Predictability, vol. 1, 1996.

[55] I. Fatkullin, E. Vanden-Eijnden, A computational strategy for multiscale systems with applications to Lorenz 96 model, J. Comput. Phys. 200 (2) (2004) 605–638.

[56] D. Burov, D. Giannakis, K. Manohar, A. Stuart, Kernel analog forecasting: multiscale test problems, Multiscale Model. Simul. 19 (2) (2021) 1011–1040.

[57] J.M. Ball, J. Carr, O. Penrose, The Becker-Döring cluster equations: basic properties and asymptotic behaviour of solutions, Commun. Math. Phys. 104 (4) (1986) 657–692.

[58] J.M. Ball, J. Carr, The discrete coagulation-fragmentation equations: existence, uniqueness, and density conservation, J. Stat. Phys. 61 (1–2) (1990) 203–234.

[59] H.R. Pruppacher, J.D. Klett, Microphysics of Clouds and Precipitation, Springer, 2010.

[60] A. Seifert, K.D. Beheng, A two-moment cloud microphysics parameterization for mixed-phase clouds. Part 1: model description, Meteorol. Atmos. Phys. 92 (2006) 45–66.

[61] I. Gibson, D.W. Rosen, B. Stucker, et al., Additive Manufacturing Technologies, vol. 17, Springer, 2014.

[62] M. Bieli, O. Dunbar, E.K. De Jong, A. Jaruga, T. Schneider, T. Bischoff, An efficient Bayesian approach to learning droplet collision kernels: proof of concept using "Cloudy", a new n-moment bulk microphysics scheme, Earth Space Sci. Open Arch. (2022) 28, https://doi.org/10.1002/essoar.10510248.1.

[63] M. Holland, I. Melbourne, Central limit theorems and invariance principles for Lorenz attractors, J. Lond. Math. Soc. 76 (2) (2007) 345–364.

[64] E. Cleary, A. Garbuno-Inigo, S. Lan, T. Schneider, A.M. Stuart, Calibrate, emulate, sample, J. Comput. Phys. 424 (2021) 109716.

[65] A. Garbuno-Inigo, F. Hoffmann, W. Li, A.M. Stuart, Interacting Langevin diffusions: gradient structure and ensemble Kalman sampler, SIAM J. Appl. Dyn. Syst. 19 (1) (2020) 412–441.

[66] O.R. Dunbar, A.B. Duncan, A.M. Stuart, M.-T. Wolfram, Ensemble inference methods for models with noisy and expensive likelihoods, SIAM J. Appl. Dyn. Syst. 21 (2) (2022) 1539–1572.

[67] E. Kalnay, Atmospheric Modeling, Data Assimilation and Predictability, Cambridge University Press, 2003.

[68] A. Javanmard, A. Montanari, et al., Debiasing the lasso: optimal sample size for Gaussian designs, Ann. Stat. 46 (6A) (2018) 2593–2622.

[69] M. Andersen, J. Dahl, Z. Liu, L. Vandenberghe, S. Sra, S. Nowozin, S. Wright, Interior-point methods for large-scale cone programming, in: Optimization for Machine Learning, MIT Press, 2011, pp. 55–83 (Chapter 3).

[70] S. Boyd, N. Parikh, E. Chu, Distributed Optimization and Statistical Learning via the Alternating Direction Method of Multipliers, Now Publishers Inc., 2011.

[71] T. Goldstein, S. Osher, The split Bregman method for l1-regularized problems, SIAM J. Imaging Sci. 2 (2) (2009) 323–343.

[72] Y. Lee, Sampling error correction in ensemble Kalman inversion, arXiv preprint, arXiv:2105.11341.

[73] J.L. Anderson, Localization and sampling error correction in ensemble Kalman filter data assimilation, Mon. Weather Rev. 140 (7) (2012) 2359–2371.

[74] X.T. Tong, M. Morzfeld, Localized ensemble Kalman inversion, arXiv preprint, arXiv:2201.10821.

[75] L. Petzold, Automatic selection of methods for solving stiff and nonstiff systems of ordinary differential equations, SIAM J. Sci. Stat. Comput. 4 (1) (1983) 136–148.

[76] A.C. Hindmarsh, Odepack, a systematized collection of ODE solvers, Sci. Comput. (1983) 55–64.

[77] S.M. Cox, P.C. Matthews, Exponential time differencing for stiff systems, J. Comput. Phys. 176 (2) (2002) 430–455.